CD89 Is a Potent Innate Receptor for Bacteria and Mediates Host Protection from Sepsis

Christian de Tymowski, Nicholas Heming, Mario D.T. Correia, Lilia Abbad, Nathalie Chavarot, Marie-Bénédicte Le Stang, Heloise Flament, Julie Bex, Erwan Boedec, Carine Bounaix, et al.

CD89 is a potent innate receptor for bacteria and mediates host protection from sepsis

Christian de Tymowski[1-4*], Nicholas Heming[1-4*], Mario D. T. Correia[5], Lilia Abbad[1-4], Nathalie Chavarot[1-4], Marie-Bénédicte Le Stang[1-4], Heloise Flament[1-4], Julie Bex[1-4], Erwan Boedec[1-4], Carine Bounaix[1-4], Rafael Soler-Torronteras[1-4], Erick Denamur[3,6], Lionel Galicier[7], Eric Oksenhendler[7], Hans Joerg Fehling[8], Fabiano Pinheiro da Silva[5], Marc Benhamou[1-4], Renato C. Monteiro[1-4,9], Sanae Ben Mkaddem[1-4]

[1]INSERM U1149, Centre de Recherche sur l'Inflammation, Paris, France; [2]CNRS ERL8252; [3]Université Paris Diderot, Sorbonne Paris Cité, Faculté de Médecine, Site Xavier Bichat, Paris, France; [4]Inflamex Laboratory of Excellence; [5]Emergency Medicine Department, Medical School, University of São Paulo, São Paulo, Brazil; [6]INSERM U1137, IAME, Paris, France; [7]Department of Clinical Immunology, Hôpital Saint-Louis, Assistance Publique Hôpitaux de Paris (APHP), Paris, France; EA3518, Université Paris Diderot Paris 7, Paris, France. [8]Institute of Immunology, University Clinics Ulm. [9]Service d'Immunologie, DHU Fire, Assistance Publique de Paris, Hôpital Bichat-Claude Bernard, Paris, France;

* C.d.T. and N.H. contributed equally to this study.

Runnig head: CD89 as innate bacteria receptor.

Lead contact: Sanae Ben Mkaddem "sanae.benmkaddem@inserm.fr" Center for Research on Inflammation, Paris Diderot Medical School (Bichat campus), INSERM U1149 & CNRS ERL8252;

Correspondence: Sanae Ben Mkaddem "sanae.benmkaddem@inserm.fr" Center for Research on Inflammation, Paris Diderot Medical School (Bichat campus), INSERM U1149 & CNRS ERL8252;

SUMMARY

Direct bacterial recognition by innate receptors is crucial for bacteria clearance. Herein, we show that the IgA receptor CD89 is a major innate receptor that directly binds bacteria independently of its cognate ligands, IgA and CRP. This binding is only partially inhibited by serum IgA and induces bacterial phagocytosis by $CD11c^+$ dendritic cells and monocytes/macrophages, suggesting a physiological role in innate host defense. Blood phagocytes from common variable immunodeficiency patients bind, internalize, and kill bacteria in a CD89-dependent manner, confirming the IgA-independence of this mechanism. *In vivo*, CD89-transgenic mice are protected in two different models of sepsis -- a model of pneumonia and the CLP polymicrobial model of infection. These data identify CD89 as a first-line innate receptor for bacterial clearance before adaptive responses can be mounted. Fc receptors may emerge as a class of innate receptors for various bacteria, with pleiotropic roles.

INTRODUCTION

Innate immunity is activated after recognition of pathogen-associated molecular patterns or structures that are not normally found in the host (Medzhitov, 2007). Phagocytes are equipped with several cell-surface receptors that recognize pathogens directly. These innate immune receptors, such as Toll-like receptors (TLRs) (Takeda and Akira, 2001), the macrophage mannose receptor, the class A scavenger receptor MARCO (Mukouhara et al., 2011) or lectin-like molecules, trigger a variety of responses depending on the receptor and the cell type (van Egmond et al., 2000): (a) internalization of the pathogen; (b) activation of microbial killing mechanisms such as production of reactive oxygen species (ROS); (c) production of inflammatory cytokines and chemokines that orchestrate the development of adaptive immunity. Dysfunction of the innate immune response may lead to sepsis (Lozano et al., 2012). Sepsis is a complex syndrome that is defined as a systemic inflammation in response to an infection and resulting in organ failures (Singer et al., 2016). Bacteria are frequent causes of sepsis and include both Gram-negative and Gram-positive pathogens (Deutschman and Tracey, 2014).

Antibody-mediated protection depends on complement and Fc receptors (FcRs) expressed predominantly by myeloid cells, subsequently initiating distinct signaling pathways (Pinheiro da Silva et al., 2008; Reth, 1989). These transmembrane receptors often contain one or more cytoplasmic immunoreceptor tyrosine-based activation motifs (ITAM). Multimeric ligation of these receptors leads to the tyrosine phosphorylation of ITAMs by Src family kinases (Abram and Lowell, 2007) leading to the recruitment of the tyrosine kinase Syk followed by cell activation (Bezbradica and Medzhitov, 2012; Humphrey et al., 2005). Several activating functions, such as phagocytosis, cytokine release, superoxide release and bacteria killing, depend on ITAM integrity (Abram and Lowell, 2007). ITAM-bearing FcRs thus emerge as key cellular determinants for antibody-mediated defenses against bacterial infections. By contrast, an ITAM-bearing FcR, the CD16A, can bind *Escherichia coli (E. coli)* directly, without requirement for opsonins, thus inducing an inhibitory signal through incomplete tyrosine phosphorylation of its ITAM and recruitment of the tyrosine phosphatase SHP-1 (Pinheiro da

Silva et al., 2007). This ITAM inhibitory (ITAMi) signaling pathway (Mkaddem et al., 2017; Blank et al., 2009; Getahun and Cambier, 2015; Hamerman and Lanier, 2006; Pasquier et al., 2005) results in the blockade of *E. coli* phagocytosis and in sepsis (Pinheiro da Silva et al., 2007). Whether this CD16A-*E. coli* interaction is unique or could be extended to other FcRs and to other bacteria and whether they could play other than deleterious roles are major questions that remain unanswered.

Here, we report that CD89 (another ITAM-bearing FcR (Monteiro and Van De Winkel, 2003) which, like CD16A, mediates dual activating/inhibitory ITAM signaling (Pasquier et al., 2005; Rossato et al., 2015)) captures Gram-negative *E. coli* on human phagocytes in the absence of its cognate ligands. Contrary to CD16A, CD89-*E. coli* interaction induces cell activation and plays a protective role in humanized CD89 transgenic mice through increased clearance and killing of these pathogens. In addition, both CD16A and CD89 bind non-opsonized Gram-positive *S. pneumoniae* (*S.p*) and both protect mice against lung infection.

RESULTS

CD89 interacts directly with Gram-positive or -negative bacteria.

As CD16A interacts directly with *E. coli* (Beppler et al., 2016; Pinheiro da Silva et al., 2007), we investigated whether another FcR distinct from FcγRs, the CD89 (Pasquier et al., 2005; Rossato et al., 2015), might similarly interact with various bacteria in the absence of opsonins. Increasing soluble recombinant CD89 (sCD89) concentrations bound dose-dependently to *S.p* and *E. coli* (Figure 1A, B). However, only a weak CD89 binding was observed with *Streptococcus pyogenes* or *S. aureus* (Figure 1C). Recently, two peptides from *E. coli* surface proteins that interact with CD16A have been identified among which WzxE (Beppler et al., 2016). To investigate if CD89 and bacteria interact through WzxE, we used WzxE$^{-/-}$ *E. coli* mutants. There was no difference in the interaction between WT or WzxE$^{-/-}$ *E. coli* and CD89 demonstrating that *E. coli* interact with CD89 independently of WzxE (Figure 1C). Moreover, the CD89-bacteria interaction apparent binding was not due to an active uptake of CD89-

detecting antibodies by bacteria because it was observed whether the bacteria were dead or alive (Figure 1D).

To examine whether transmembrane CD89 can bind bacteria, we took advantage of *in vitro* binding capacity of labelled *S.p* or *E. coli* to bone marrow derived macrophages (BMM) isolated from CD89 transgenic animals (Launay et al., 2000) in the absence of exogenous CD89 ligands, IgA and CRP. *S.p* bound 4 fold more to BMM derived from $CD89^{Tg}$ animals than to BMM obtained from littermates (Figure 1E). Similarly, *E. coli* bound 2 fold more to $CD89^{Tg}$ BMM (Figure 1F). Binding of both *S.p* and *E. coli* to $CD89^{+}$ BMM, but not to BMM from littermates, was markedly inhibited by MIP8a, an anti-human CD89 blocking mAb, (Figure 1G and H) demonstrating the involvement of the IgA-binding site on CD89 for these interactions. For *S.p*, full inhibition of receptor interaction required higher concentration of MIP8a or sCD89 (500-1000 µg/ml) (Figure S1A-B). Moreover, sCD89 blocked *S.p* or *E. coli* interactions not only with $CD89^{+}$ cells, but also, to some extent, with $CD89^{-}$ cells suggesting that sCD89 binding to bacteria may disturb bacteria binding to other innate receptors (Figure 1G, H). Similar to BMM, CD89 expression on CD11c+ Bone Marrow Dendritic Cells (BMDC) increased bacteria phagocytosis which was significantly inhibited by MIP8a (Figure S1C).

Bacteria-CD89 interaction on mouse macrophages induces cell activation, bacteria phagocytosis and bacterial killing that are dependent on the FcRγ chain.

Interaction of $CD89^{Tg}$ BMM with *S.p,* in the absence of cognate CD89 ligands, resulted in a strong increase in the mRNA expression and protein production of IL-6, TNF-α but not of IL-1. *E. coli* induced the mRNA expression and protein production of IL-6 and TNF-α whereas for IL-1, despite of no difference in mRNA expression, an increase in IL1-β protein production was observed in $CD89^{Tg}$ BMM (Figure 2A-B and Figure S1D-E). Caspase-1-dependent posttranscriptional modifications of IL-1β may explain these differences as reported by others (Bakema et al., 2015). To determine whether ITAM-dependent signalling is required for these responses, we used BMM from a transgenic mouse expressing a genetically modified version of the CD89, the $CD89_{R209L}$, bearing a Leu instead of an Arg at position 209 in the

transmembrane region (R209L). This mutant receptor cannot associate with the ITAM-bearing FcRγ signalling subunit (Launay et al., 1999). $CD89_{R209L}{}^{Tg}$ BMM bound to both bacteria species similarly to $CD89^{Tg}$ cells, indicating that the CD89-FcRγ interaction is not essential for bacteria binding (Figure S2). However, CD89-mediated cytokine production was completely dependent on the associated ITAM-bearing FcRγ subunit, as $CD89_{R209L}{}^{Tg}$ BMM failed to upregulate IL-6 and TNFα secretion (Figure 2A and B). To evaluate the role of innate receptors and FcRs on the differential bacteria capture, we assessed by flow cytometry the membrane expression on BMM of TLRs 1, 2, 3, 4, 5, 6, 8, Mannose receptor, MARCO, CD16, CD32 and CD64 (Figure S3 A-C). Membrane expression of TLRs, FcRs, Mannose receptor and MARCO showed no significant difference between wild-type and $CD89^{Tg}$ BMM whether before or after stimulation, showing that they are not responsible for the difference in bacteria capture observed between these cells.

To examine the phagocytic role of CD89 following bacteria interaction, we performed *E. coli* phagocytosis assay using the pHrodo dye labelling system. Cells from $CD89^{Tg}$ mice internalized significantly more *E. coli* than cells from littermates and this was inhibited by MIP8a $F(ab')_2$ and sCD89 in a dose-dependent manner (Figure 2C). This indicates that direct *E. coli* binding to CD89 results in bacteria phagocytosis and delivery to phago-lysosomes in absence of IgA opsonins. Next, we assessed whether this led to increased ROS production and bacterial killing. Live *S.p* or *E. coli* induced a robust upregulation of ROS production by $CD89^{Tg}$ BMM that was dependent on the FcRγ chain since it was fully absent in $CD89_{R209L}{}^{Tg}$ cells where it reached levels comparable to the ones observed in cells from littermates (Figure 2D). Killing of *S.p* or *E. coli* by $CD89^{Tg}$ BMM was significantly higher compared to that by BMM derived from littermate or $CD89_{R209L}{}^{Tg}$ animals (Figure 2E). Live bacteria number decreased by a 100 fold in $CD89^{Tg}$ BMM cultures as compared to littermate and $CD89_{R209L}{}^{Tg}$ cells within 2h of infection. To explore the signaling pathway involved, we analyzed the recruitment of Syk to CD89 following stimulation of BMM obtained from $CD89^{Tg}$ or littermate mice by either *S.p* or *E. coli.* Bacteria-CD89 interaction resulted in a sustained recruitment of Syk (lasting for a

minimum of 2 h) to the FcRγ-associated CD89, while $CD89_{R209L}{}^{Tg}$ BMM failed to induce such recruitment (Figure 2F). A Syk recruitment to CD89, but not of SHP-1 (Figure S4A), following bacteria stimulation was also observed in cultured human blood monocytes which was inhibited by the addition of sCD89 (Figure S4B). Together, these results indicate that bacteria-CD89 interaction results in the induction of FcRγ ITAM signaling pathway leading to stable Syk recruitment and cell activation with bacteria phagocytosis and killing.

IgA-deficient CVID phagocytes mediate phagocytosis, ROS production and bacteria killing through CD89 interaction.

To further demonstrate that CD89-bacteria interaction occurs independently of IgA, we examined human blood phagocytes from healthy donors (HD) and from severe CVID patients who are totally deficient in plasma IgA (Table S1). CD89 expression on blood monocytes and neutrophils was maintained (Figure 3A), and even significantly increased (Figure S5A and B), in CVID patients as compared to HD. *S.p* and *E. coli* binding to cells from CVID or HD was dependent on CD89 as they were inhibited by MIP8a $F(ab')_2$ and by non-specific human IgA (devoid of anti-bacteria antibody activity, ns-IgA) (Figure 3B and S5C). As expected, specific hIgA (plasma derived IgA, pd-IgA) increased significantly the phagocytosis (Figure S5D). Therefore, although pd-IgA can serve as an opsonin, binding of *S.p* and *E. coli* to CD89 does not require IgA.

To confirm the phagocytic and activating role of native, human CD89 towards bacteria independently of IgA, we performed *E. coli* pHrodo phagocytosis assay followed by anti-bacterial responses in blood monocytes purified from CVID patients. Culture-derived macrophages from CVID patient monocytes efficiently phagocytosed labelled *E. coli* similarly to HD cells (Figure 3C). Moreover, MIP8a $F(ab')_2$ markedly decreased bacteria phagocytosis confirming that CD89-bacteria interaction was functional even in absence of human IgA. This was associated with efficient cytokine and ROS productions (Figure 3D and E), which were inhibited by MIP8a $F(ab')_2$. Finally, cultured-derived macrophages from CVID patients performed bacterial killing in a similar manner as cells from healthy individuals (Figure 3F). Of

note, MIP8a F(ab')$_2$ blocked more than 80% of the cell activation suggesting that, while blocking the interaction between the bacteria and CD89, it induces at the same time an inhibition of cell activation by scavenger and innate immune receptors in agreement with others (Watanabe et al., 2011).

Taken together, these findings indicate that CD89-bacteria interaction results in essential FcR activating functions (phagocytosis, cytokine and ROS production and bacteria killing) which are preserved in human blood phagocytes from IgA deficient CVID patients suggesting that CD89 may play a direct protective role against *E. coli* and *S.p* infections in absence of IgA.

Role of CD89-bacteria interaction under physiological conditions.

To address the physiological role of CD89-bacteria interaction, we examined whether it was prevented by competition with physiological concentration of ns-IgA. Both *S.p* and *E. coli* binding were inhibited by ns-IgA (which does not present any anti-bacterial activity) in a dose-dependent manner (Figure 4A) demonstrating that bacteria binding on CD89 was hindered by IgA binding to the CD89 D1 domain. However, this inhibition was partial and reached a plateau of 80% inhibition above 700µg/ml IgA allowing a remaining significant proportion of sCD89 to bind bacteria despite physiological concentrations of IgA (up to 2 mg/ml). As expected, bacteria-CD89 binding was increased in the presence of IgA displaying anti-bacteria antibody activity acting as opsonins (Figure 4B). To further determine whether the remaining binding of bacteria to CD89 observed in the presence of physiologic concentration of IgA could be functionally relevant we explored bacteria capture in the presence of 2 mg/ml ns-IgA or of MIP8a F(ab)'$_2$ fragment. The strong increase in bacteria capture observed in CD89^{Tg} BMM was significantly reduced in the presence of physiological concentrations of ns-IgA or in the presence of MIP8a F(ab)'$_2$. However, it remained increased by 50 to 100% as compared to bacteria capture by BMM derived from littermate animals (Figure 4C) thus confirming CD89 as a potent innate receptor for bacteria. Monocytes/macrophages are not the only immune cells expressing CD89. Among these other CD89$^+$ cells, a subset of immature dendritic cells, notably epidermal Langerhans cells, can capture bacteria in sites that have low IgA antibody

concentrations (Geissmann et al., 2001; Pasquier et al., 2004). Similar to BMM, CD89 expression on CD11c+ BMDC significantly enhanced bacteria phagocytosis as compared to that of BMDC from littermates (Figure 4D and E). This enhancement remained strong (around a 100% increase) even under physiological concentrations of ns-IgA or with MIP8a F(ab)'$_2$ (Figure 4D, Figure S1C and 5C). Altogether, these experiments suggest that CD89-bacteria direct interaction can be effective in the interior milieu and hence may play a physiological role for the host.

CD89-bacteria interaction protects against mortality in two sepsis models.

To investigate the *in vivo* role of the direct interaction between bacteria and CD89 on bacterial clearance, we performed experimental pneumonia caused by intranasal infection with *S.p*, a Gram-positive coccus (Lu et al., 2008). CD89^{Tg} mice exhibited significantly lower mortality following infection relative to littermates (Figure 5A). The number of live *S.p* in the lungs of CD89^{Tg} animals was 100 fold lower 48h post-inoculation as compared to littermates (Figure 5B) in agreement with the increased bactericidal/phagocytic CD89-dependent activity in phagocytes from the former animals as described above. CD89^{Tg} mice showed both less interstitial and peribronchiolar infiltration as well as less alveolitis (Figure 5C and D). Alveolar spaces were infiltrated by monomorphic cells, but these cells were in markedly higher number in non-transgenic littermates. Moreover, CD89^{Tg} mice expressed higher local mRNA levels of the inflammatory cytokine IL-1 6h after bacteria inoculation, but this early inflammation resolved more rapidly with a level of IL-1 mRNA showing a trend to lower levels in CD89^{Tg} animals 48h post-infection as compared to littermates (Figure 5E). By contrast, IL-6 level significantly increased in littermate compared to transgenic mice 6h and 48h after infection. This suggests that the level IL-6 is associated with the severity of sepsis. However, the level of TNF-α mRNA was identical in the two groups at 6h and 48h.

To extend the protective role of CD89 to polymicrobial infections, we assessed the consequences of CD89 expression in a severe model of peritonitis induced by CLP. As in the pneumonia model, the CD89^{Tg} mice were significantly protected from sepsis (Figure 5F). The

peritoneum of $CD89^{Tg}$ mice contained a lower number of total bacteria, *E. coli* and *Enterococcus* (the major strains identified by MALDI-TOF) than littermates after CLP (Figure 5G-I). $CD89^{Tg}$ mice expressed early and transient IL-1 and TNF-α responses in the peritoneum post-CLP as compared with the delayed responses observed in wild-type animals (Figure 5J). These early responses were associated with markedly lower mortality rates. Taken together, these results indicate that following CLP, CD89 triggered by gut-residing bacteria induces a more efficient phagocytosis together with a better controlled and rapid pro-inflammatory response resulting in decreased bacteria number in the peritoneum and in more effective protection of the host. As in *S.p* model, IL-6 increased only in littermate compared to $CD89^{Tg}$ mice 48h post-CLP, confirming the deleterious role of IL-6 in sepsis and the level of this cytokine may be a biomarker of sepsis severity.

To confirm that CD89 can protect against sepsis induced by $Gram^-$ bacteria, we used the sepsis model of intraperitoneal *E.coli* injection. As in the pneumonia and CLP models, $CD89^{Tg}$ mice were protected to a great extent from sepsis (Figure S6A). The peritoneum of $CD89^{Tg}$ animals contained a lower number of bacteria than littermates after 48h of infection (Figure S6B). $CD89^{Tg}$ mice expressed early and transient IL-1 and TNF-α responses in the peritoneum post-infection as compared with the delayed responses observed in wild-type animals (Figure S6C).

CD89 protection against sepsis is dependent on the FcRγ chain.

As the CD89-associated FcRγ chain was mandatory for the CD89-dependent bactericidal activity of phagocytes (cf above-described data), we performed similar infection experiments using $CD89_{R209L}{}^{Tg}$ mice to determine whether FcRγ was also required for the protection observed *in vivo*. No difference in mortality with littermates was observed in intranasal infection with *S.p* or after CLP (Figure 6A and F) indicating that bacteria interaction with $CD89_{R209L}$ is not protective. This was confirmed by similar bacteria number colonizing the infected tissues, similar alveolite score, similar cytokine responses and tissue injury between littermate and $CD89_{R209L}{}^{Tg}$ mice (Figure 6B-E and F-H).

CD89 protects against sepsis in the absence of CD16 during Gram-positive infections.

As mouse CD16 interacts directly with *E. coli* (Figure S6D) and aggravates sepsis in the CLP model through the induction of ITAMi signal (Pinheiro da Silva et al., 2007), we examined whether it could interact also with *S.p*. CD16 readily interacted with these bacteria (Figure S6D) and protected mice against *S.p* pneumonia (Figure 6I), in contrast to its deleterious action in the CLP model (Figure S6E) demonstrating that CD16 plays opposite roles in sepsis depending on the type of bacteria and/or organs involved. We then explored whether CD89 could further protect mice beyond what has been observed in CD16-KO mice. In the pneumonia model CD89 was protective regardless of the presence of CD16, demonstrating that its action did not rely on CD16 (Figure 6I). In the CLP-induced sepsis, CD89 provided a slightly supplemental protection (albeit not reaching statistical significance) to that observed in the absence of CD16 (Figure S6E). Therefore, CD89 is a reliable receptor in immune defence against infection and may counter-balance the CD16-ITAMi inhibitory signal that is deleterious in the CLP model of acute peritonitis.

CD89-mediated protection against sepsis is independent of CRP and of anti-bacteria IgA antibodies.

Since CRP is a known ligand for CD89 that could serve as an opsonin (Du Clos and Mold, 2011), we took advantage of CRP-KO mice (Teupser et al., 2011), and backcrossed them to CD89^{Tg} mice. Similar to what we described above for WT and CD89^{Tg} mice, a significant increase in survival rates was obtained when the CD89 gene was introduced in the CRP-KO background (Figure 7A and D). This was associated with significant decreases in live bacteria counts in lung and peritoneal cavities of CD89^{Tg}CRP-KO mice as compared to CRP-KO mice (Figure 7B and E). This protection was associated with a robust early inflammation (at 6h) followed by an efficient resolution of inflammation (at 48h) as measured by the local level of cytokine mRNA or proteins (IL-1, TNF-α and IL-6) (Figure 7C and F). Phagocytosis assays showed significant increase in bacteria phagocytosis in BMM from CD89^{Tg}CRP-KO when compared to CRP-KO which was inhibited by addition of MIP8a F(ab')$_2$ (Figure 7G and H),

confirming the CRP-independent protective role of CD89. To exclude the role of mouse IgA antibodies in this protection through a putative interaction with human CD89 (mouse IgA interacts weakly with human CD89 (Berthelot et al., 2012)), we measured IgA anti-bacteria antibody levels at 48h and day 7 after infections. 48h after infection, when a significant increase in survival in $CD89^{Tg}$CRP-KO mice was already detectable ($p<0.02$; see Figure 7A and D), no anti-bacteria IgA was detected yet in the serum of both models of infected mice (intranasal infections and CLP) (Figure 7I).

Since the pentraxin CRP binds and activates CD89 (Lu et al., 2011), we also investigated the effect of the absence of CRP on bacteria binding to CD89. Since BMM can produce CRP (Li et al., 2012) we used BMM derived from WT or $CRP^{-/-}$ mice on $CD89^{Tg}$ background. The bacteria binding assay showed that both *S.p* and *E. coli* interact with CD89 independently of CRP and these interactions were inhibited by MIP8a anti-CD89 $F(ab')_2$ (Figure S7A). In the CLP model, the level of CRP from $CD89^{Tg}$ and WT mice slightly increased in the peritoneal exudate and doubled in serum 6h after infection reaching between 20 and 25 µg/ml without any difference between the two strains (Figure S7B and C). To formally exclude the role of CRP in the CD89-mediated host protection, we explored whether 25 µg/ml CRP increased *E. coli* phagocytosis by $CD89^{+}$ monocytes. This concentration had no effect on *E. coli* phagocytosis, whereas (as expected) high level of CRP (200µg/ml) increased it (Figure S7D). These results demonstrate that neither a different modulation of CRP expression by CD89 nor CRP itself is required for CD89-dependent protection against infection.

Additional analyses were performed to further determine whether mouse IgA could be involved in the CD89-mediated protection. At steady state, monocytes isolated from WT or $CD89^{Tg}$ mice bound similarly mouse IgA (Figure S7E). As well, BMM isolated from $CD89^{Tg}$ mice bound poorly non-specific mouse IgA but, as a positive control, bound readily non-specific human IgA. The low binding of mouse IgA was not increased by the presence of bacteria (Figure S7F). To explore the effects of mouse IgA-CD89 interaction, serum IgA binding to BMM was compared between serum collected at day 1 and day 7 from mice subjected to infection. IgA

binding increased similarly at day 7 compared to day 1 in BMM from WT and CD89Tg mice (Figure S7G). Therefore, no difference in mouse IgA binding could be detected between WT and CD89^{Tg} monocytes and no bacteria-specific mouse IgA was detected early after infection, confirming that the CD89-dependent protection observed in our experimental settings did not involve mouse IgA. Taken together, these results identify CD89 as an innate immune receptor that could play a crucial role in host protection during the early phase of bacterial infections.

DISCUSSION

Our results demonstrate that CD89 binds both Gram+ and Gram- bacilli in a direct, opsonin-independent manner, resulting in increased protection against infection. In addition to IgA, CD89 also binds CRP, an acute-phase protein (Lu et al., 2011). Binding of CRP to CD89 on a distinct binding site from that of IgA, induces activation of both macrophages and neutrophils, which play a major role in the innate response to infection. However, neither IgA nor CRP account for the CD89 interaction with bacteria described here, as our *in vitro* and *ex vivo* studies were performed in the absence of both proteins and were confirmed *in vivo* in the absence of detectable IgA opsonins and of CRP.

Many innate immune receptors are involved in bacteria recognition by macrophages, including TLRs, MARCO, various lectins and the IgG receptor CD16A. The fact that the sole additional presence of CD89 is capable *in vitro* to, at least, double the capture of bacteria (see Figure 1), double the production of cytokines and of ROS and decrease by a 100 fold the number of bacteria surviving phagocytosis (see Figure 2), reveals CD89 as a major player in antibacterial defense. These effects were confirmed in *in vivo* models where the number of bacteria collected in tissue 48h after infection was reduced by a 100-fold in CD89^{Tg} as compared to WT mice together with a powerful increase in cytokine production and survival (see Figure 5). However, this protection (survival) was lower than expected from the 90-99% reduction of bacterial load observed in CD89^{Tg} mice. This suggests that in our infection protocols the bacterial loads were in large excess to what is necessary to induce sepsis and that in infections with lower bacterial loads the protection provided by CD89 could be more drastic. Whereas

mouse IgA bind poorly to CD89 and thus should not compete with bacteria for CD89 binding, in humans, serum IgA inhibit bacteria binding to CD89 (see Figure 3). However, human serum IgA does not completely block bacteria binding to CD89, as observed in the ELISA experiments depicted in Figure 3. Hence, a significant number of free CD89 would remain available for bacteria capture allowing a physiological role of this interaction notably by Langerhans cells which are usually located in sites with low IgA concentration. The fact that no bacteria-specific mouse IgA antibodies were detected in CD89^{Tg} and in CD89^{Tg}CRP-KO mice early (48h) after infections, i.e. at a time when CD89-dependent protection was already strongly effective in these mice, indicate that not only CD89 is a receptor for bacteria but also that it may play an important role in innate immune responses against infections before adaptive responses take place (see Figure 7I).

In our sepsis models, CD89 proved efficient in reducing the bacteria burden and in improving the survival of the animals. One can propose that the improved capture and killing of the bacteria, together with the increased early inflammatory reaction that we observed, may favor a robust and rapid mobilization of the innate immune system that can contain more efficiently bacteria invasion before it could get out of hand. This acceleration of the inflammatory reaction would also contribute to the CD89-dependent resolution of inflammation.

The direct involvement of CD89 in innate immune responses adds a layer to the various functions of this receptor. Immune responses are controlled by a balance of antagonistic signals. This balance prevents tissue damage by ensuring the return of activated cells to their resting state. The CD89-IgA pair plays a major role in host defense as well as a dual role in immunity by mediating either activating or inhibitory responses. This dual activity of CD89 is mirrored by the dual activity of serum IgA, which may exert either an anti- or a pro-inflammatory activity (Ben Mkaddem et al., 2013; Rossato et al., 2015). Anti-inflammatory signals are generated by CD89 upon binding of monomeric IgA, whereas pro-inflammatory CD89-dependent responses are induced by IgA immune complexes. The latter initiate multiple biological processes, including phagocytosis and antibody-dependent cell-mediated

cytotoxicity, leading to targeted bacteria lysis (Bakema and van Egmond, 2011). CD89 cross-linking by its ligand can also promote cell activation resulting in the release of cytokines, inflammatory mediators and superoxide anion. Furthermore, pro-inflammatory cytokines induce CD89 expression on Kupffer cells of $CD89^{Tg}$ mice, leading to increased clearance of mouse IgA-coated bacteria (van Egmond et al., 2000). It has thus been proposed that interactions between serum IgA and CD89 on Kupffer cells may provide a 'second line of defense' in mucosal immunity, by eliminating invasive bacteria entering through the portal circulation. However, mouse IgA have very low affinity for human CD89 (Berthelot et al., 2012) which, in agreement with our observations, would argue in favor of a direct binding of bacteria to CD89 on Kupffer cells. This mechanism of defense would promote bacteria capture and subsequent macrophage activation through CD89 before the generation of specific IgA is completed. This would reinforce a prompt innate immune response before highly proliferative microbes overwhelm the immune system.

Although the frequency of infections is a hallmark of immunodeficiencies, there are few studies comparing the frequency of infections between selective IgAD and CVID patients and unfortunately no data, to our knowledge, comparing different bacterial strains. It has been reported, however, that IgAD patients present less severe pulmonary infections when compared to IgAD associated with IgG subclass deficiency (Bjorkander et al., 1985). In a recent study it has been reported that while prolonged very low levels of IgG and/or IgM are associated with a heightened risk of infections, selective IgAD appears to be better tolerated by most patients (Furst, 2009). Our data on blood phagocytes from CVID patients with no IgA but reconstituted for IgG and IgM revealed that CD89 is upregulated and functional as it is able to mediate bacteria internalization and killing. These findings are in agreement with previous observations supporting the residual ability of IgAD patients to fight infections.

Interestingly, and in line with our study, CD89 expression and activation are increased in human blood phagocytes following bacterial infection, together with an increased expression and association of FcRγ with CD89 (Chiamolera et al., 2001). Moreover, LPS up-regulates

CD89 expression on blood monocytes (Shen et al., 1994). The fact that bacteria or bacterial products can increase CD89 expression is in phase with our present data that CD89-mediated protection in mice occurs also in absence of specific IgA antibodies at day 2 which led us to postulate that CD89 acts as an innate immune receptor in the early phase of infection when individuals are not yet armed with specific antibodies. On the other hand in the late phase of infection once the IgA antibody responses are established, CD89 direct binding to the bacteria may further increase CD89 crosslinking by providing additional anchoring sites for capture of opsonized bacteria, enhancing ITAM signaling, phagocytosis and bacterial clearance. The existence of two means of bacteria capture by CD89 (IgA-dependent and IgA-independent) which may cooperate during the late phase of infection when an IgA response has taken place, emphasizes the importance of this receptor in immunity.

Taking advantage of the balance between activating and inhibitory immune responses, micro-organisms are able to subvert the human immune system, inducing inhibitory signals in order to survive (Van Avondt et al., 2015). We previously observed that *E. coli* subvert CD16A signaling in order to evade the host immune system, by inducing a potent ITAMi inhibitory signal involving SHP-1, leading to sepsis. In contrast, in *S.p* infection, CD16A was required for protection. Further structural studies of the binding of the various bacteria species to CD16A will be necessary to elucidate the basis for these opposite signals. Interestingly and in contrast to CD16A, binding both of *E. coli* and of *S.p* to CD89 led to the recruitment of Syk, bacteria phagocytosis and controlled inflammation as evidenced by the resolution of IL-1 production at 48h in the pneumonia and CLP models and in the enhanced survival of $CD89^{Tg}$ mice. Of note, whereas both CD89 and CD16A are functionally associated with the FcRγ adaptor, their genes are located in different chromosomes and there is no homology between the extracellular domains of these receptors (Monteiro and Van De Winkel, 2003) suggesting that differences in their extracellular domains may indeed account for their different behaviour in the presence of *E. coli*. Additional studies will be necessary to shed light on this puzzling contrast. However, while CD16-KO mice were protected against CLP-mediated sepsis, $CD89^{Tg}$ mice (which still

express CD16) were as protected as CD16-KO mice arguing in favour of a different bacteria-binding site on these receptors. Hence, it is expected that non-opsonized bacteria bind both CD16A and CD89 on phagocytes. Our results show that the activating signal generated by CD89 can overcome the inhibitory signal generated by CD16A in the CLP model.

Altogether, our results suggest that the CD89 fulfils an innate protective role against non-opsonized bacteria immediately after infection in the absence of specific IgA and in the presence of the low basal levels of CRP. This role would further progress taking advantage of rising CRP levels that would provide CRP opsonins for CD89 binding and would finally evolve to an immune adaptive role once the adaptive IgA immune response has kicked in. Thus, the CD89 should be considered as a receptor with a complex and dynamic plasticity encompassing that of the immune response to infection.

Although WzxE protein from *E. coli* interacts with CD16 (Beppler et al., 2016), it failed to interact with CD89 as receptor binding to WzxE-/- mutant *E. coli* remained unchanged. This result argues in favor of a different *E. coli* binding site. Thus, it remains unknown which molecular determinants of the bacterial cell surface of *E. coli, S. Aureus* and *S.p* interact with CD89.

Several other questions arise from our study. For instance, what are the respective molecular determinants that allow bacteria binding to CD16A and to CD89 and are they shared between bacteria species and between these FcR? Can these FcR bind other pathogens such as viruses, parasites or yeasts? Whatever the answers to these questions that future will provide, our study, by demonstrating that at least two different FcR are able to bind two different (Gram-positive and Gram-negative) non-opsonized bacteria species with various outcomes (protection or aggravation), allows one to contemplate whether FcRs can now emerge as a class of innate receptors and to speculate that this may have been their prime function early in evolution.

Overall, our findings expand the spectrum of signals able to activate cells through FcRs and open avenues for the treatment of bacterial infections such as therapeutic interventions aimed

at stimulating CD89 expression to boost anti-pathogen responses. This study uncovers the importance of the ITAM-bearing CD89 in innate immunity and in sepsis.

ACKNOWLEDGMENTS

The authors thank the confocal microscopy image facility. This work was supported by grants from ANR JC (ANR-17-CE17-0002-01), DIM1HEALTH "action financée par la Région Ile-de-France", and from LabEx Inflamex (ANR-11-IDEX-0005-02). R.C.M. was supported by « Equipe » program of the Fondation pour la recherche médicale (FRM). C.D.T was supported by FRM (41482). The authors thank Dr. Cedric Vonarburg and CSL Behring for providing human monomeric plasma derived IgA (pdIgA). We are indebted to the patients and healthy volunteers who participated in the study.

AUTHOR CONTRIBUTIONS

Contribution: C.T., N.H., M.T., L.A., N.C., E.B., J.B., R.S.T. and C.B. performed experiments and analyzed data; H.J.F. generated CRP-KO mice; L.G. and E.O. provided human samples and analyzed data; E.D., M.B. and R.C.M. contributed to analysis of the data and editing of the manuscript; S.B.M. designed the research, analyzed data and wrote the manuscript.

DECLARATION OF INTERESTS

The authors declare no competing interests.

Figure Legends

Figure 1. Recombinant soluble CD89 receptor interacts directly with bacteria

(A-B) Dose dependent binding of soluble recombinant CD89 (sCD89) to fixed *S.p* (A) or *E. coli* (B). Binding to albumin (Alb) was used as a control.

(C) Comparison of sCD89 binding to various types of fixed bacteria.

(D) Interaction of sCD89 with live (green bar) *vs* fixed (black bars) 10^6 *E. coli* or 10^6 *S. p.*

(E-F) Bacteria binding to BMM grown from CD89 transgenic mice ($CD89^{Tg}$) or from littermates by confocal laser scanning microscopy. Right panels, quantification of the bindings (n=4). All data are presented as mean ± SEM. **p<0.01. t-test.

(G-H) Bacteria binding to BMM isolated from $CD89^{Tg}$ mice or from littermates in the presence or absence of the anti-CD89 blocking antibody, MIP8a $F(ab')_2$ (10µg/ml), or of sCD89 (500µg/ml) analyzed by flow cytometry. MFI: Mean of Fluorescence Intensity. Data are presented as mean ± SEM; n=5. *p<0.05, **p<0.01. t-test.

See also Figure S1.

Figure 2. Bacteria-CD89 interaction on mouse cells induces activating ITAM signalling leading to inflammatory cytokine production, bacterial phagocytosis and killing.

(A-B) IL-6, TNF-α and IL-1 production in the supernatant of BMM obtained from $CD89^{Tg}$ and $CD89_{R209L}$ transgenic mice, and littermate controls. Cells were incubated for 16h in the presence of *E. coli* or *S.p* and cytokines in the supernatants were measured by ELISA. All data are presented as mean ± SEM. n=3. *p<0.05, **p<0.01.t-test.

(C) Confocal analysis of *E. coli*/pHrodo phagocytosis by BMM obtained from $CD89^{Tg}$ mice compared to littermates in the presence or absence of MIP8a $F(ab)'_2$ or sCD89 in a dose-dependent manner (100 to 800µg/ml). Left panels: representative images. Right panels: quantification. Data are presented as mean ± SEM. n=3. ***p<0.001. t-test.

(D) ROS production over 30 minutes by littermate, $CD89^{Tg}$ and $CD89_{R209L}$ transgenic BMM stimulated by live *S.p* (left panel) or *E. coli,* (right panel) measured by confocal. All data are presented as mean ± SEM. n=15. **p<0.01. t-test.

(E) Quantification of bacterial survival after 2h of incubation with BMM from $CD89^{Tg}$, $CD89_{R209L}{}^{Tg}$, and littermate mice. Data are presented as mean ± SEM; n=3. ***p<0.001. t-test.

(F) Induction of CD89-ITAM signaling by *S.p* or *E. coli.* After incubation of BMM from littermate, $CD89^{Tg}$ or $CD89_{R209L}{}^{Tg}$ mice with 10^6 CFU of *S.p* (upper panels) or *E. coli* (lower panels) for the indicated times, co-immunoprecipitated (IP) proteins by A77 anti-CD89 mAb (top) and total

proteins (bottom) were analyzed by immunoblotting (IB) using rabbit polyclonal anti-Syk antibody.

See also Figure S1-S4

Figure 3. IgA-deficient CVID phagocytes mediate phagocytosis, ROS production and bacterial killing through CD89 interaction.

(A) Representative plots of CD89 expression on blood monocytes isolated from healthy donors (HD) (left panel) and from CVID patients (right panel) using PE-conjugated anti-CD89 antibody and its isotype control.

(B) Binding of *S.p* or of *E. coli* to blood monocytes from HD (purple symbols) or from CVID patients (red symbols) in the presence of monomeric IgA (500 µg/ml) or of MIP8a $F(ab')_2$ (10µg/ml). All data are presented as mean ± SEM. n=4. ***p<0.001. t-test.

(C) Phagocytosis of *E. coli*/pHrodo by human blood monocytes/macrophages isolated from HD or from CVID patients. Left panels: representative images. Scale bars: 200 µm. Right histogram: quantification (n=3). All data are presented as mean ± SEM. ns: not significant.

(D) IL-6, TNF-α and IL-1 production in the supernatant of monocytes obtained from CVID patients. Cells were incubated for 16h in the presence of *E. coli* or *S.p* in the presence or the absence of MIP8a $F(ab')_2$ fragment (500µg/ml) and cytokines in the supernatants were measured by ELISA. All data are presented as mean ± SEM. n=3. *p<0.05, **p<0.01, ****p<0.0001. t-test.

(E) Production of ROS in response to co-incubation of HD or CVID human monocytes with *S.p or E. coli* in the presence or absence of MIP8a $F(ab')_2$. Experiments were performed as in Figure 3D. All data are presented as mean ± SEM. n=3. *p<0.05; ns: not significant. t-test.

(F) Bacteria survival after incubation with HD or CVID human monocytes for 2h in the presence or absence of MIP8a $F(ab')_2$ as in Figure 3E (n=3). Data are presented as mean ± SEM. n=4. All data are presented as mean ± SEM. **p<0.01; ns: not significant.

See also Figure S5 and table S1.

Figure 4. Role of CD89-bacterial interaction under physiological conditions.

(A) Competitive ELISA assays between sCD89 and *S.p* (blue line) or *E. coli* (red line), and ns-IgA.

(B) Competitive ELISA assays between sCD89 and *S.p* (blue line) or *E. coli* (red line), and pd-IgA.

(C) Bacterial phagocytosis by BMM obtained from $CD89^{Tg}$ mice (left panel) compared to littermates (right panel). Bacterial were allowed to be phagocytized by BMM from the indicated mice in the presence or absence of ns-IgA at physiological concentration (2mg/ml) or MIP8a $F(ab)'_2$ fragment (500µg/ml). Cells were washed and analysed by flow cytometry. Data are presented as mean ± SEM. n=3. *<0.05, ***p<0.001. t-test.

(D) *S.p* (left panel) or *E. coli* (right panel) phagocytosis by BMDC obtained from $CD89^{Tg}$ mice compared to littermates. Bacterial were allowed to be phagocytozed by BMDC from the indicated mice in the presence or absence of ns-IgA at physiological concentration (2mg/ml). Cells were washed and analysed by flow cytometry. Data are presented as mean ± SEM. n=3. *<0.05, ***p<0.0001. t-test.

(E) Representative images of *E. coli* (blue) and CD11c (red) staining by BMDC derived from $CD89^{Tg}$ or Wild-Type (WT) mice captured by imaging flow cytometry (scale bar = 5 µm) and the percentages of the bacteria phagocytosis score.

See also Figure S1C and S5C.

Figure 5. CD89-bacteria interaction protects against infection-related mortality in mice.

(A) Survival of $CD89^{Tg}$ (red line) and littermates (black line) after intranasal inoculation (at time 0) with *S. pneumonia* (n=25). Kaplan-Meier curves and the log-rank test were used to compare mortality rates. All data are presented as mean ± SEM. *p<0.05.

(B) Decreased lung contents of *S.p* in CD89 transgenic as compared to littermate. All data are presented as mean ± SEM. n=8. ***p<0.001. t-test.

(C) HE staining of lung sections from representative $CD89^{Tg}$ and littermate animals after intranasal infections. Scale bars = 200 µm.

(D) Alveolitis score invasion by monomorphic inflammatory cells. All data are presented as mean ± SEM. n=6. ***p<0.001.t-test.

(E) mRNA expression of cytokines (IL1, TNF-α and IL-6) was assessed by quantitative reverse transcriptase–polymerase chain reaction of 5 independent lung tissue RNA samples collected 6 and 48h after intranasal infection. mRNA levels were normalized to β-actin mRNA levels. All data are presented as mean ± SEM. n=6. *p<0.05. ns: not significant. t-test.

(F) Increased survival of $CD89^{Tg}$ mice (red line, n=26) compared to littermates (black line, n=22) after CLP. Kaplan-Meier curves and the log-rank test were used to compare mortality rates. All data are presented as mean ± SEM. **p<0.01.

(G-I) 48h after CLP, peritoneal fluids were counted for total bacteria (G), *E. coli* (H) and *Enterococcus* (I) in $CD89^{Tg}$ mice and in littermate. All data are presented as mean ± SEM. *p<0.05, **p<0.01, ***p<0.001. t-test.

(J) IL-1, TNF-α and IL-6 levels in peritoneal lavage assessed by ELISA 6 and 48h after CLP. All data are presented as mean ± SEM. n=3. *p<0.05, ns: not significant. t-test.

See also Figure S6A-C.

Figure 6. CD89 protects against sepsis through the FcRy chain-dependent pathway.

(A) Increased survival of $CD89^{Tg}$ animals after lung infection by intranasal inoculation with *S.p* compared to $CD89_{R209L}^{Tg}$ or littermates. Kaplan-Meier curves and the log-rank test were used to compare mortality rates. All data are presented as mean ± SEM. n=10. *p<0.05. ns: not significant. t-test.

(B) Decreased lung counts of *S.p* in $CD89^{Tg}$ as compared to $CD89_{R209L}^{Tg}$ or littermates (n=5). All data are presented as mean ± SEM. *p<0.05; ns: not significant. t-test.

(C) HE staining of lung sections from representative $CD89_{R209L}^{Tg}$ mice and littermates after intra-nasal infections. Scale bars = 200 µm.

(D) Alveolitis score invasion by monomorphic inflammatory cells. All data are presented as mean ± SEM. *p<0.05; ns: not significant. t-test.

(E) mRNA expression of IL1, TNF-α and IL-6 in RNA samples collected 6h after intranasal inoculation from lung tissue of distinct mice. Cytokine mRNA levels were normalized to β-actin mRNA levels as indicated in Figure 5E. Data are presented as mean ± SEM; n=4. *p<0.05, ns: not significant. t-test.

(F) Increased survival of $CD89^{Tg}$ mice (n=10) compared to $CD89_{R209L}{}^{Tg}$ or littermates (n=10) after CLP. Kaplan-Meier curves and the log-rank test were used to compare mortality rates. Data are presented as mean ± SEM. **p<0.01.

(G) After 48h of CLP, peritoneal fluid counts of bacteria were less numerous in the peritoneal fluid of $CD89^{Tg}$ mice than in those from $CD89_{R209L}{}^{Tg}$ or littermate animals (n=5). All data are presented as mean ± SEM. **p<0.01; ns: not significant. t-test.

(H) IL-1, TNF-α and IL-6 levels in peritoneal lavage assessed by ELISA 6h after CLP. Data are presented as mean ± SEM; n=5. *p<0.05, **p<0.01, ns: not significant. t-test.

(I) Survival rates of CD16 KO, CD16 KO-$CD89^{Tg}$, $CD89^{Tg}$ and littermate mice after intranasal *S.p* infection (I). Kaplan-Meier curves and the log-rank test were used to compare mortality rates. Data are presented as mean ± SEM. ***p<0.001.

See also Figure S6D-E.

Figure 7. CD89 protection against sepsis is independent of CRP and IgA antibodies during early phase of infection.

(A) Increased survival of $CD89^{Tg}$CRP-KO animals after intranasal infection with *S.p* compared to CRP-KO mice (n=12 per group). $CD89^{Tg}$ mice and their littermate were used as controls of the experiment. Kaplan-Meier curves and the log-rank test were used to compare mortality rates. All data are presented as mean ± SEM.

(B) Decreased lung counts of *S.p* in $CD89^{Tg}$CRP-KO at 48h as compared to CRP-KO mice (n=4). All data are presented as mean ± SEM. **p<0.01. t-test.

(C) Expression of cytokine mRNA (IL1, TNF-α and IL-6) was assessed by Q-PCR of independent lung tissue RNA samples collected 6 and 24h after intranasal infection. Cytokine mRNA levels were normalized to β-actin mRNA levels as indicated in Figure 5E (n=4). All data are presented as mean ± SEM. *p<0.05, **p<0.01. t-test.

(D) Increased survival of $CD89^{Tg}$CRP-KO (n=10) compared to CRP-KO mice (n=10) after CLP. Kaplan-Meier curves and the log-rank test were used to compare mortality rates. $CD89^{Tg}$ mice and their littermate were used as controls of the experiment. All data are presented as mean ± SEM.

(E) Peritoneal fluid counts of bacteria 48h after CLP (n=4). All data are presented as mean ± SEM. **p<0.01. t-test.

(F) IL-1, TNF-α and IL-6 levels in peritoneal lavage assessed by ELISA 6 and 48h after CLP (n=4). All data are presented as mean ± SEM. *p<0.05, **p<0.01. t-test.

(G) Phagocytosis of *S.p* (left panel) and *E. coli* (right panel) and its inhibition (H) after incubation with BMM isolated from $CD89^{Tg}$CRP-KO or CRP-KO in the presence of MIP8a anti-CD89 $F(ab')_2$. All data are presented as mean ± SEM. *p<0.05, **p<0.01. t-test.

(I) Measurement of mouse IgA antibodies against the indicated bacteria at 48 or 168h after *S.p* infection (left panel) or CLP (right panel) in $CD89^{Tg}$ or $CD89^{Tg}$CRP-KO mice. For all panels, data are presented as mean ± SEM.

See also Figure S7.

STAR★METHODS

CONTACT FOR REAGENT AND RESOURCE SHARING

Further information and request for resources and reagents should be directed to and will be fulfilled by the Lead Contact, Sanae Ben Mkaddem (sanae.benmkaddem@inserm.fr).

EXPERIMENTAL MODEL AND SUBJECT DETAILS

Subjects

Eight patients with common variable immunodeficiency disorders (CVID) based on the criteria used for the diagnosis of CVID consistent with the European Society for

Immunodeficiencies/Pan-American Group for Immunodeficiency criteria (Conley et al., 1999) were included in this study. Patients studied were selected with IgG replacement for the present study. Serum IgA levels were < 0.05 g/l (Table S1). The study was approved by the French ethic committees" Comité Consultatif pour la protection des personnes dans la recherché biomedicale, Ile de France-Paris-St ANTOINE)", the approval number is 04579 and all human participants provided written informed consent. Blood from seven healthy donors was obtained from the Etablissement Français du Sang (Saint Louis hospital).

Animals

Female C57BL/6 $CD89^{Tg}$ mice expressing the wild-type human CD89 on monocytes/macrophages under the control of the CD11b promoter as well as mice expressing the R209L mutant of CD89 under control of the same promoter ($CD89_{R209L}{}^{Tg}$) all aged 8-12 weeks were used, as previously described (Kanamaru et al., 2007; Launay et al., 2000). As mice do not express homologues of CD89, non-transgenic littermates served as negative controls. Of note, mouse IgA does not bind effectively CD89 (Pleass et al., 1999);(Berthelot et al., 2012). CD16-KO mice were from the Jackson Laboratory and the $CD89^{Tg}$CD16-KO were obtained by backcrossing of CD16-KO and $CD89^{Tg}$. C-reactive protein (CRP) knock-out mice have been previously described (Teupser et al., 2011). All strains were maintained at the animal facility of Bichat Medical School. All experiments were performed in accordance with the French Council of Animal Care guidelines and national ethical guidelines of Paris-Nord Animal Care Committee (Animal Use Protocol number C2EA-121).

METHOD DETAILS

Pneumonia and cecal ligation and puncture models

Pneumonia was induced by intranasal administration of 5.10^5 CFU of *S. pneumoniae Pn3* (ATCC-6303, Manassas, USA) in mice under isoflurane anaesthesia (Baxter, France). Paraffin-embedded lung sections were obtained and stained with H&E for morphological analysis. Peritonitis was induced by CLP as described (Pinheiro da Silva et al., 2007; Rittirsch et al., 2009). Briefly, mice were anesthetized using ketamine and xylasine (Virbac, France).

After anaesthesia, the abdomen was shaved, and the cecum exposed through a 1-cm midline incision. The cecum was ligated between the 3rd and 4th vascular arcade with a 4-0 silk suture (Ethicon, France) and punctured twice with a 21-gauge needle. Recovery was facilitated by placing mice on a heated pad. Blood was collected by cardiac puncture, and haematological parameters were monitored using a MS9 analyser (Melet Schloesing, France). Time to death was recorded during the following 7 days, when surviving mice were euthanized.

Cells, reagents and antibodies

In mouse experiments, bone-derived mouse macrophages (BMM) were obtained after a 7-day culture of bone marrow cells from 8 to 12-week-old mice in the presence of colony-stimulating factor1 (R&D system, France). In *ex-vivo* human blood cell experiments, peripheral blood mononuclear cells (PBMC) were first isolated by using Ficoll gradients followed by a negative selection for monocytes using Dynabeads™ Untouched™ Human Monocytes Kit (Invitrogen, France). Monocytes were cultured in RPMI supplemented with glutamate (Invitrogen, France) and 10% foetal bovine serum (Invitrogen, France) for 5 days to generate macrophages.

BMDCs were generated from 6-8 week-old wild-type and $CD89^{Tg}$ mice. Briefly, a cell suspension was prepared from BM obtained from femurs and tibias. After lysing red blood cells, whole BM cells (2 × 106 cells/mL) were cultured in RPMI 1640 medium in six-well flat bottom plates (Orange Scientific, Braine-l'Alleud, Belgium) at 37 °C, 5% CO2, supplemented with 10% fetal calf serum (FCS), 2 mM L-glutamine, 100 U/mL penicillin G, 100 mg/mL streptomycin, 30 ng/mL reconstructive mouse GM-CSF (Peprotech, Rocky Hill, USA) and 20 ng/mL reconstructive mouse IL-4 (Peprotech, Rocky Hill, USA). Cells were incubated for 24 h. Plates were then gently swirled and the medium containing non-adherent cells was removed and replaced with nutrient medium as described above. Supplemented medium was replaced every three days. Cell differentiation was assessed by flow-cytometry staining using anti-CD11c (N418) and anti-CD11b (M1/70) (BD Biosciences; each at 2 µg/ml).

Anti-CD89 (clone A59)-phycoerythrin (PE) conjugate was purchased from Becton Dickinson. Unconjugated MIP8a anti-CD89 was purchased from (ABD Serotec) and digested by pepsin

to generate $F(ab')_2$ fragments as described (Aloulou et al., 2012). Human monomeric plasma derived IgA (pd-IgA) from one thousand healthy donors was kindly provided by CSL behring. Of note, the pd-IgA preparation was purified from the same batch that contain IVIg antibodies reacting to different bacteria which was efficient against infection in CIVD patients (Lucas et al., 2010). Non-specific human monomeric IgA (ns-IgA) was purchased from (MP biomedicals, France).

The *Escherichia coli* (*E. coli*-K12, Strain SMG 123 (PTA-7555)), *Staphylococcus aureus* subsp. aureus Rosenbach (*S. aureus*, ATCC® 25923™), *Streptococcus pyogenes* Rosenbach (*S. pyogenes*, ATCC® 19615™) and *Escherichia coli*-K12 WzxE (Coli genetic stock center, Yale university) were used for sCD89-bacteria interaction assays shown in figure 1C.

Flow cytometry

Expression of CD89 was quantified on cells using flow cytometry. Cells were preincubated or not with 100 µg human IgG to block FcγRs for 15 min before incubation with labeled mAbs or irrelevant mAb for 30 min at 4°C. After washing, cells were analyzed by FACSfortessa flow cytometer (Becton Dickinson). Results were analyzed using the FlowJo software (Ashland, OR, USA). Receptor expression was represented by the ratio of mean fluorescence intensity (MFI) of receptor/ MFI of isotype control.

Imaging flow cytometry

BMDCs were generated as described above. BMDCs were washed and incubated, in the absence of foetal bovine serum, with Texas-red labeled *E. coli* () for 2h at 37°C. Cells were fixed with PFA 2% then anti-mouse CD11c (BD Biosciences) were used for membrane staining. BMDCs were gated as Singlets cells/Focus high/CD11c high. *E. coli* staining (Texas-Red) was determined for each BMDCs as the ratio of the geometric mean of their *E. coli* intensity on the mean BMDCs CD11c FMO (Fluorescence Minus One) intensity. Phagocytosis scores were determined using CD11c staining as a membrane marker and *E. coli* staining as the probe. All analyses were performed using the ImageStream X Mark II imaging flow cytometer and the IDEAS v6 software (AMNIS) (Figure 4).

Protein expression on BMM membrane

Protein expression of TLRs and of MARCO was quantified on BMM using flow cytometry. Anti TLR antibodies were obtained from Imgenex (Clinisciences, Nanterre, France), including anti-TLR1 phycoerythrin (PE) conjugate, anti-TLR2 Fluorescein isothiocyanate (FITC) conjugate anti-TLR3 phycoerythrin (PE) conjugate, anti-TLR4 Fluorescein isothiocyanate (FITC) conjugate, anti-TLR5 phycoerythrin (PE) conjugate, anti-TLR6 phycoerythrin (PE) conjugate, anti-TLR8 phycoerythrin (PE) conjugate. Anti-MARCO antibodies were obtained from Santa Cruz (Heidelberg, Germany). Isotype controls were obtained from Becton Dickinson. BMM were stained with anti-extracellular antibodies for 30 minutes at 4°C. A total of 10000 viable PBMC were collected using BD FACSDiva Software by flow cytometry (FACSCanto II, Becton Dickinson, France). Results were analyzed using the FlowJo software (Ashland, OR, USA). TLR expression is represented by the ratio of mean fluorescence intensity (MFI) of TLR / MFI of isotype control.

Bacteria and microbiological culture

Serotype 3 *S. pneumoniae*, was grown in Todd Hewitt Broth media (Becton Dickinson, France) supplemented by 0.5% yeast extract (Becton Dickinson, France) at 37°C, to midlog phase. Strain K-12 MG1655 is a laboratory-derived commensal *E. coli* strain. It belongs to the A phylogenetic group and has no resistance to antibiotics or virulence factors. The K-12 *E. coli* strain was grown in Luria–Bertani (Becton Dickinson, France) broth at 37°C, to midlog phase. *Streptococcus pyogenes* (CIP 56.41T, Pasteur Institute, France) was grown in Todd Hewitt Broth media supplemented by 0.5% yeast extract at 37°C, to midlog phase. Bacteria were pelleted by centrifugation (16,000 x g for 10 minutes), washed twice in endotoxin-free PBS (Invitrogen). Bacteria concentration was determined spectrophotometrically (A600) and then confirmed by plating serially diluted bacteria on respectively soy-based blood agar plates (Becton Dickinson, France) and Luria–Bertani agar plates.

Bacterial invasion count

Pneumonia model: lungs were harvested and then homogenized with a tissue blender (Ultra-Turrax T25, Fisher Scientific, France) in one millilitre of 0.9% sodium chloride during 1 minute. Bacterial counts were determined by plating serial dilutions of the homogenate on soy-based blood agar plates (Becton Dickinson, France).

Cecal ligation and puncture model: peritoneal fluid was serially diluted, and subsequently spread on Luria–Bertani agar plates (Becton Dickinson, France) and bacteria-selective agar plates. Plates were incubated in aerobic conditions for 1 day. *E. coli* selective medium was Drigalski agar (Becton Dickinson, France), *Enterococcus* were detected and quantified using Columbia CNA agar (Becton Dickinson, France) and identified by MALDI-TOF technique. Results are expressed as log CFU/organ.

Bacterial binding and phagocytosis assays

10^6 BMM were washed and incubated, in the absence of foetal bovine serum, with Texas-red labeled *E. coli* (Molecular Probes) or 10^7 CFU 5,6-carboxyfluorescein succinimidyl ester (FAM-SE; Molecular Probes, Thermo Fisher, France) labeled *S. pneumoniae* (Martinez et al., 1999) for 30 minutes at 4°C for the binding assays or 37°C for the phagocytosis assays, respectively. The staining of WGA (4 µg/ml in PBS) was performed on fixed cells with 4% of PFA and after bacteria binding or phagocytosis assays. Slides were mounted and examined by confocal laser scanning microscopy with a CLSM-510-META microscope (Carl Zeiss, France).

For *E. coli* phagocytosis assay in BMM derived from $CD89^{Tg}$ animals or littermates, we used the pHrodo dye labelling system, in which pHrodo™ label of internalized bacteria dramatically increase in fluorescence at the acidic pH found in phago-lysosomes giving a good quantitative index of bacteria phagocytosis.

Bacterial killing

To measure intracellular bacterial killing, in the absence of foetal bovine serum, we incubated live *E. coli* (ATCC no. 25922) with cells (10^7 bacteria per $5x10^5$ cells) at 37 °C for 30 min. We removed unbound bacteria by differential centrifugation (Leijh et al., 1979) and suspended the

pellets in gentamicin solution (100 µg/ml from Sigma-Aldrich, St. Louis, MO), which we incubated for 2h at 37 °C to kill any extracellular bacteria. After rinsing in PBS, cells were either lysed by incubation on ice with 0.5% Triton X-100 for 10 min or incubated at 37 °C for 30 and 60 min before lysis under the same conditions (Leijh et al., 1979). We counted the surviving bacteria on selective agar plates.

Confocal laser scanning microscopy

The production of reactive oxygen species by BMM was measured by imaging microscopy. BMM were plated on Lab-Tek chambered coverglass slides (Thermo Fisher scientific, France) and loaded with 50 µM DCFH-DA (Invitrogen, France) for 30 minutes. Cells were then rinsed and stimulated with 10^{-8} of fMLF. After excitation at 488 nm, the green fluorescence of DCF was measured by confocal laser scanning microscopy with CLSM-510-META microscope (Carl Zeiss, France) equipped with a cell culture chamber at 37°C, under 5% CO_2 atmosphere.

ROS production assay on PMN by chemiluminescence

After isolation, PMNs were suspended in Hank's Balanced Salt Solution (Life technologies, France) to reach a concentration of 10^6 cells per ml and left to rest for 30 minutes at room temperature. fMLF (Sigma-Aldrich, France) and Luminol (Sigma-Aldrich, France) were diluted 1:100 in Hank's Balanced Salt Solution and kept on ice. Luminol (Sigma-Aldrich, France) was protected from light by aluminium foil. Five hundred µl of the solution containing PMNs were added to each of 6 tubes followed by the addition of Luminol and 10 minutes incubation at 37°C in the chamber of a luminometer (Berthold–Biolumat LB937, France). Changes in chemiluminescence were then measured over 30 minutes after stimulation with *E. coli*, *S. pneumoniae* or with fMLF.

Immunoprecipitation and immunoblotting

Cells were solubilized in lysis buffer containing 1% Nonidet P-40, 0.1% sodium dodecyl sulfate (SDS) (Sigma-Aldrich, France). For immunoprecipitation, cell lysates were incubated with A77 anti-CD89 mAb and immunoprecipitated overnight at 4°C with Protein G-Sepharose beads

(GE Healthcare, France) as described (Ben Mkaddem et al., 2014). Samples were resolved by SDS–10% polyacrylamide gel electrophoresis, transferred onto nitrocellulose membranes and immunoblotted with rabbit anti-Syk (Santa Cruz Biotechnology, USA) or rabbit anti–SHP-1 (Santa Cruz Biotechnology, USA) antibodies followed by goat anti–rabbit IgG (GE Healthcare, France) coupled to horseradish peroxidase. Membranes were developed by enhanced chemical luminescence treatment (Amersham Biosciences, France).

Production of soluble proteins and antibodies

Soluble CD89 was expressed and produced in lytic baculovirus/insect cell expression systems (home-made as described (Berthelot et al., 2012)). Mouse IgG1 anti-CD89 mAbs (clones A3 and A77) were produced and purified in our laboratory as described (Monteiro et al., 1992). A3 and A77 were used for ELISA.

ELISA

Regarding cytokine and chemokine assays, mouse TNF-α, IL-1 and IL-6 levels were measured by ELISA, following the manufacturer's instructions (R&D Systems, France). Regarding binding assays, plates were coated overnight with 10^5, 10^6, 10^7, 10^8 chemically killed bacteria in 100 µL of sterile PBS. Wells were then blocked with milk 2% for 2h. Recombinant soluble CD89 in PBS was incubated for 2h. After washing, the biotinylated A3 mAb anti-CD89 was added followed by streptavidin alkaline phosphatase (Becton Dickinson, France). The reaction was developed by adding the alkaline phosphatase substrate (Sigma-Aldrich, France) for 1 hour and measured at 405nm. As a negative control, plates coated with only albumin were used. Competitive ELISA assays between human IgA, bacteria and soluble recombinant CD89 were undertaken using human IgA (MP Biomedicals, France) and human IgG (TEGELINE, LFB Biomedical, les ULIS France) as a control. Briefly, 50µg/ml of sCD89 was incubated with different concentrations of serum IgA for 30 minutes. Then the complex was added on plates coated with 10^6 bacteria and incubated for another 2h at 37°C. After washing,

the biotinylated A3 mAb anti-CD89 was added followed by streptavidin alkaline phosphatase (Becton Dickinson, France) and the reaction was developed as described above.

Real-time PCR

RNA purification from homogenized kidneys was performed by using RNAble (Eurobio). cDNA was obtained by reverse transcription using Moloney murine leukaemia virus reverse transcriptase (Invitrogen, France). Samples were analyzed by real-time PCR with TaqMan® Gene Expression Master Mix (Invitrogen, France). Respective primers and probe sequences, which were purchased from Eurofins, are shown in Supplemental table 2. Gene quantification was performed using a Chromo4 Real-Time PCR Detection System (Bio-Rad Laboratories, France). Data were normalized to β-actin mRNA values.

QUANTIFICATION AND STATISTICAL ANALYSIS

All data were obtained using cells from at least three independent culture preparations or at least three independent animals per genotype. Repeats for experiments and statistical tests carried out are given in the figure legends as N numbers and refer to number of cells unless otherwise stated. Statistical analysis was performed using the Graphpad Prism v7.00 software (GraphPad Software, Inc., La Jolla, CA, USA). Mann-Whitney tests were performed for between-group comparisons. Survival differences were determined using the Kaplan-Meier method and the Log-rank test. All tests were two-tailed. (not significant [ns], $p>0.05$; * $p<0.05$; ** $p<0.01$; *** $p<0.001$).

References

Abram, C.L., and Lowell, C.A. (2007). The expanding role for ITAM-based signaling pathways in immune cells. Science's STKE : signal transduction knowledge environment *2007*, re2.

Aloulou, M., Ben Mkaddem, S., Biarnes-Pelicot, M., Boussetta, T., Souchet, H., Rossato, E., Benhamou, M., Crestani, B., Zhu, Z., Blank, U., *et al.* (2012). IgG1 and IVIg induce inhibitory ITAM signaling through FcgammaRIII controlling inflammatory responses. Blood *119*, 3084-3096.

Bakema, J.E., Tuk, C.W., van Vliet, S.J., Bruijns, S.C., Vos, J.B., Letsiou, S., Dijkstra, C.D., van Kooyk, Y., Brenkman, A.B., and van Egmond, M. (2015). Antibody-opsonized bacteria evoke an inflammatory dendritic cell phenotype and polyfunctional Th cells by cross-talk between TLRs and FcRs. J Immunol *194*, 1856-1866.

Bakema, J.E., and van Egmond, M. (2011). The human immunoglobulin A Fc receptor FcalphaRI: a multifaceted regulator of mucosal immunity. Mucosal immunology *4*, 612-624.

Ben Mkaddem, S., Hayem, G., Jonsson, F., Rossato, E., Boedec, E., Boussetta, T., El Benna, J., Launay, P., Goujon, J.M., Benhamou, M.*, et al.* (2014). Shifting FcgammaRIIA-ITAM from activation to inhibitory configuration ameliorates arthritis. J Clin Invest *124*, 3945-3959.

Ben Mkaddem, S., Rossato, E., Heming, N., and Monteiro, R.C. (2013). Anti-inflammatory role of the IgA Fc receptor (CD89): from autoimmunity to therapeutic perspectives. Autoimmunity reviews *12*, 666-669.

Beppler, J., Mkaddem, S.B., Michaloski, J., Honorato, R.V., Velasco, I.T., de Oliveira, P.S., Giordano, R.J., Monteiro, R.C., and Pinheiro da Silva, F. (2016). Negative regulation of bacterial killing and inflammation by two novel CD16 ligands. European journal of immunology *46*, 1926-1935.

Berthelot, L., Papista, C., Maciel, T.T., Biarnes-Pelicot, M., Tissandie, E., Wang, P.H., Tamouza, H., Jamin, A., Bex-Coudrat, J., Gestin, A.*, et al.* (2012). Transglutaminase is essential for IgA nephropathy development acting through IgA receptors. The Journal of experimental medicine *209*, 793-806.

Bezbradica, J.S., and Medzhitov, R. (2012). Role of ITAM signaling module in signal integration. Current opinion in immunology *24*, 58-66.

Bjorkander, J., Bake, B., Oxelius, V.A., and Hanson, L.A. (1985). Impaired lung function in patients with IgA deficiency and low levels of IgG2 or IgG3. N Engl J Med *313*, 720-724.

Blank, U., Launay, P., Benhamou, M., and Monteiro, R.C. (2009). Inhibitory ITAMs as novel regulators of immunity. Immunological reviews *232*, 59-71.

Chiamolera, M., Launay, P., Montenegro, V., Rivero, M.C., Velasco, I.T., and Monteiro, R.C. (2001). Enhanced expression of Fc alpha receptor I on blood phagocytes of patients with gram-negative bacteremia is associated with tyrosine phosphorylation of the FcR-gamma subunit. Shock *16*, 344-348.

Conley, M.E., Notarangelo, L.D., and Etzioni, A. (1999). Diagnostic criteria for primary immunodeficiencies. Representing PAGID (Pan-American Group for Immunodeficiency) and ESID (European Society for Immunodeficiencies). Clin Immunol *93*, 190-197.

Deutschman, C.S., and Tracey, K.J. (2014). Sepsis: current dogma and new perspectives. Immunity *40*, 463-475.

Du Clos, T.W., and Mold, C. (2011). Pentraxins (CRP, SAP) in the process of complement activation and clearance of apoptotic bodies through Fcgamma receptors. Curr Opin Organ Transplant *16*, 15-20.

Furst, D.E. (2009). Serum immunoglobulins and risk of infection: how low can you go? Semin Arthritis Rheum *39*, 18-29.

Geissmann, F., Launay, P., Pasquier, B., Lepelletier, Y., Leborgne, M., Lehuen, A., Brousse, N., and Monteiro, R.C. (2001). A subset of human dendritic cells expresses IgA Fc receptor (CD89), which mediates internalization and activation upon cross-linking by IgA complexes. J Immunol *166*, 346-352.

Getahun, A., and Cambier, J.C. (2015). Of ITIMs, ITAMs, and ITAMis: revisiting immunoglobulin Fc receptor signaling. Immunological reviews *268*, 66-73.

Hamerman, J.A., and Lanier, L.L. (2006). Inhibition of immune responses by ITAM-bearing receptors. Science's STKE : signal transduction knowledge environment *2006*, re1.

Humphrey, M.B., Lanier, L.L., and Nakamura, M.C. (2005). Role of ITAM-containing adapter proteins and their receptors in the immune system and bone. Immunological reviews *208*, 50-65.

Kanamaru, Y., Arcos-Fajardo, M., Moura, I.C., Tsuge, T., Cohen, H., Essig, M., Vrtovsnik, F., Loirat, C., Peuchmaur, M., Beaudoin, L.*, et al.* (2007). Fc alpha receptor I activation induces leukocyte recruitment

and promotes aggravation of glomerulonephritis through the FcR gamma adaptor. European journal of immunology *37*, 1116-1128.

Launay, P., Grossetete, B., Arcos-Fajardo, M., Gaudin, E., Torres, S.P., Beaudoin, L., Patey-Mariaud de Serre, N., Lehuen, A., and Monteiro, R.C. (2000). Fcalpha receptor (CD89) mediates the development of immunoglobulin A (IgA) nephropathy (Berger's disease). Evidence for pathogenic soluble receptor-Iga complexes in patients and CD89 transgenic mice. The Journal of experimental medicine *191*, 1999-2009.

Launay, P., Patry, C., Lehuen, A., Pasquier, B., Blank, U., and Monteiro, R.C. (1999). Alternative endocytic pathway for immunoglobulin A Fc receptors (CD89) depends on the lack of FcRgamma association and protects against degradation of bound ligand. J Biol Chem *274*, 7216-7225.

Leijh, P.C., van den Barselaar, M.T., van Zwet, T.L., Daha, M.R., and van Furth, R. (1979). Requirement of extracellular complement and immunoglobulin for intracellular killing of micro-organisms by human monocytes. J Clin Invest *63*, 772-784.

Li, M., Liu, J.T., Pang, X.M., Han, C.J., and Mao, J.J. (2012). Epigallocatechin-3-gallate inhibits angiotensin II and interleukin-6-induced C-reactive protein production in macrophages. Pharmacol Rep *64*, 912-918.

Lozano, R., Naghavi, M., Foreman, K., Lim, S., Shibuya, K., Aboyans, V., Abraham, J., Adair, T., Aggarwal, R., Ahn, S.Y.*, et al.* (2012). Global and regional mortality from 235 causes of death for 20 age groups in 1990 and 2010: a systematic analysis for the Global Burden of Disease Study 2010. Lancet *380*, 2095-2128.

Lu, J., Marjon, K.D., Marnell, L.L., Wang, R., Mold, C., Du Clos, T.W., and Sun, P. (2011). Recognition and functional activation of the human IgA receptor (FcalphaRI) by C-reactive protein. Proceedings of the National Academy of Sciences of the United States of America *108*, 4974-4979.

Lu, J., Marnell, L.L., Marjon, K.D., Mold, C., Du Clos, T.W., and Sun, P.D. (2008). Structural recognition and functional activation of FcgammaR by innate pentraxins. Nature *456*, 989-992.

Lucas, M., Lee, M., Lortan, J., Lopez-Granados, E., Misbah, S., and Chapel, H. (2010). Infection outcomes in patients with common variable immunodeficiency disorders: relationship to immunoglobulin therapy over 22 years. J Allergy Clin Immunol *125*, 1354-1360 e1354.

Martinez, J.E., Romero-Steiner, S., Pilishvili, T., Barnard, S., Schinsky, J., Goldblatt, D., and Carlone, G.M. (1999). A flow cytometric opsonophagocytic assay for measurement of functional antibodies elicited after vaccination with the 23-valent pneumococcal polysaccharide vaccine. Clinical and diagnostic laboratory immunology *6*, 581-586.

Medzhitov, R. (2007). Recognition of microorganisms and activation of the immune response. Nature *449*, 819-826.

Mkaddem, S.B., Murua, A., Flament, H., Titeca-Beauport, D., Bounaix, C., Danelli, L., Launay, P., Benhamou, M., Blank, U., Daugas, E.*, et al.* (2017). Lyn and Fyn function as molecular switches that control immunoreceptors to direct homeostasis or inflammation. Nat Commun *8*, 246.

Monteiro, R.C., Cooper, M.D., and Kubagawa, H. (1992). Molecular heterogeneity of Fc alpha receptors detected by receptor-specific monoclonal antibodies. J Immunol *148*, 1764-1770.

Monteiro, R.C., and Van De Winkel, J.G. (2003). IgA Fc receptors. Annual review of immunology *21*, 177-204.

Mukouhara, T., Arimoto, T., Cho, K., Yamamoto, M., and Igarashi, T. (2011). Surface lipoprotein PpiA of Streptococcus mutans suppresses scavenger receptor MARCO-dependent phagocytosis by macrophages. Infection and immunity *79*, 4933-4940.

Pasquier, B., Launay, P., Kanamaru, Y., Moura, I.C., Pfirsch, S., Ruffie, C., Henin, D., Benhamou, M., Pretolani, M., Blank, U., *et al.* (2005). Identification of FcalphaRI as an inhibitory receptor that controls inflammation: dual role of FcRgamma ITAM. Immunity *22*, 31-42.

Pasquier, B., Lepelletier, Y., Baude, C., Hermine, O., and Monteiro, R.C. (2004). Differential expression and function of IgA receptors (CD89 and CD71) during maturation of dendritic cells. J Leukoc Biol *76*, 1134-1141.

Pinheiro da Silva, F., Aloulou, M., Benhamou, M., and Monteiro, R.C. (2008). Inhibitory ITAMs: a matter of life and death. Trends in immunology *29*, 366-373.

Pinheiro da Silva, F., Aloulou, M., Skurnik, D., Benhamou, M., Andremont, A., Velasco, I.T., Chiamolera, M., Verbeek, J.S., Launay, P., and Monteiro, R.C. (2007). CD16 promotes Escherichia coli sepsis through an FcR gamma inhibitory pathway that prevents phagocytosis and facilitates inflammation. Nature medicine *13*, 1368-1374.

Pleass, R.J., Dunlop, J.I., Anderson, C.M., and Woof, J.M. (1999). Identification of residues in the CH2/CH3 domain interface of IgA essential for interaction with the human fcalpha receptor (FcalphaR) CD89. J Biol Chem *274*, 23508-23514.

Reth, M. (1989). Antigen receptor tail clue. Nature *338*, 383-384.

Rittirsch, D., Huber-Lang, M.S., Flierl, M.A., and Ward, P.A. (2009). Immunodesign of experimental sepsis by cecal ligation and puncture. Nature protocols *4*, 31-36.

Rossato, E., Ben Mkaddem, S., Kanamaru, Y., Hurtado-Nedelec, M., Hayem, G., Descatoire, V., Vonarburg, C., Miescher, S., Zuercher, A.W., and Monteiro, R.C. (2015). Reversal of Arthritis by Human Monomeric IgA Through the Receptor-Mediated SH2 Domain-Containing Phosphatase 1 Inhibitory Pathway. Arthritis Rheumatol *67*, 1766-1777.

Shen, L., Collins, J.E., Schoenborn, M.A., and Maliszewski, C.R. (1994). Lipopolysaccharide and cytokine augmentation of human monocyte IgA receptor expression and function. J Immunol *152*, 4080-4086.

Singer, M., Deutschman, C.S., Seymour, C.W., Shankar-Hari, M., Annane, D., Bauer, M., Bellomo, R., Bernard, G.R., Chiche, J.D., Coopersmith, C.M., *et al.* (2016). The Third International Consensus Definitions for Sepsis and Septic Shock (Sepsis-3). Jama *315*, 801-810.

Takeda, K., and Akira, S. (2001). Roles of Toll-like receptors in innate immune responses. Genes to cells : devoted to molecular & cellular mechanisms *6*, 733-742.

Teupser, D., Weber, O., Rao, T.N., Sass, K., Thiery, J., and Fehling, H.J. (2011). No reduction of atherosclerosis in C-reactive protein (CRP)-deficient mice. J Biol Chem *286*, 6272-6279.

Van Avondt, K., van Sorge, N.M., and Meyaard, L. (2015). Bacterial immune evasion through manipulation of host inhibitory immune signaling. PLoS pathogens *11*, e1004644.

van Egmond, M., van Garderen, E., van Spriel, A.B., Damen, C.A., van Amersfoort, E.S., van Zandbergen, G., van Hattum, J., Kuiper, J., and van de Winkel, J.G. (2000). FcalphaRI-positive liver Kupffer cells: reappraisal of the function of immunoglobulin A in immunity. Nature medicine *6*, 680-685.

Watanabe, T., Kanamaru, Y., Liu, C., Suzuki, Y., Tada, N., Okumura, K., Horikoshi, S., and Tomino, Y. (2011). Negative regulation of inflammatory responses by immunoglobulin A receptor (FcalphaRI) inhibits the development of Toll-like receptor-9 signalling-accelerated glomerulonephritis. Clin Exp Immunol *166*, 235-250.

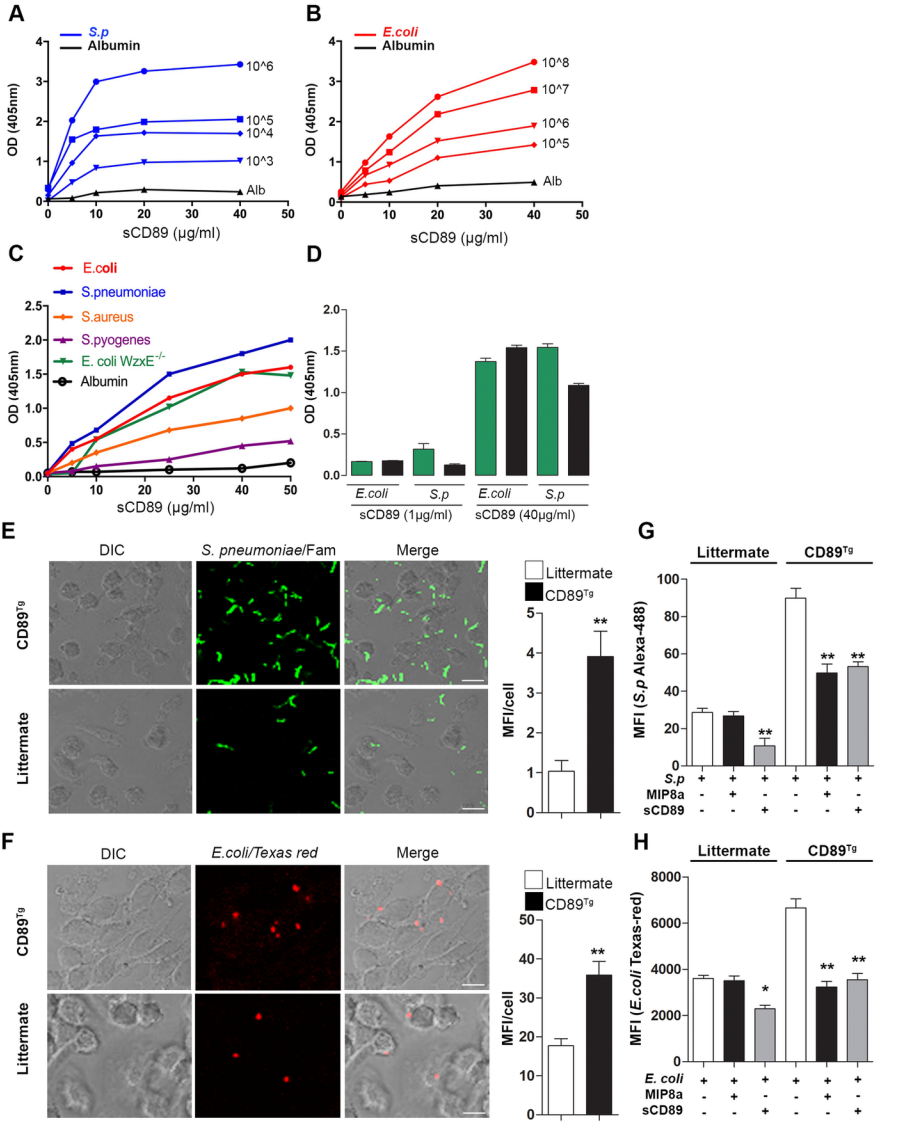
A
S.p
Albumin
10^6
10^5
10^4
10^3
Alb
OD (405nm)
sCD89 (μg/ml)
B
E.coli
Albumin
10^8
10^7
10^6
10^5
Alb
OD (405nm)
sCD89 (μg/ml)
C
E.coli
S.pneumoniae
S.aureus
S.pyogenes
E. coli WzxE-/-
Albumin
OD (405nm)
sCD89 (μg/ml)
D
OD (405nm)
E.coli
S.p
E.coli
S.p
sCD89 (1μg/ml)
sCD89 (40μg/ml)
E
DIC
S. pneumoniae/Fam
Merge
CD89Tg
Littermate
Littermate
CD89Tg
MFI/cell
F
DIC
E.coli/Texas red
Merge
CD89Tg
Littermate
Littermate
CD89Tg
MFI/cell
G
Littermate
CD89Tg
MFI (S.p Alexa-488)
S.p
MIP8a
sCD89
H
Littermate
CD89Tg
MFI (E.coli Texas-red)
E. coli
MIP8a
sCD89

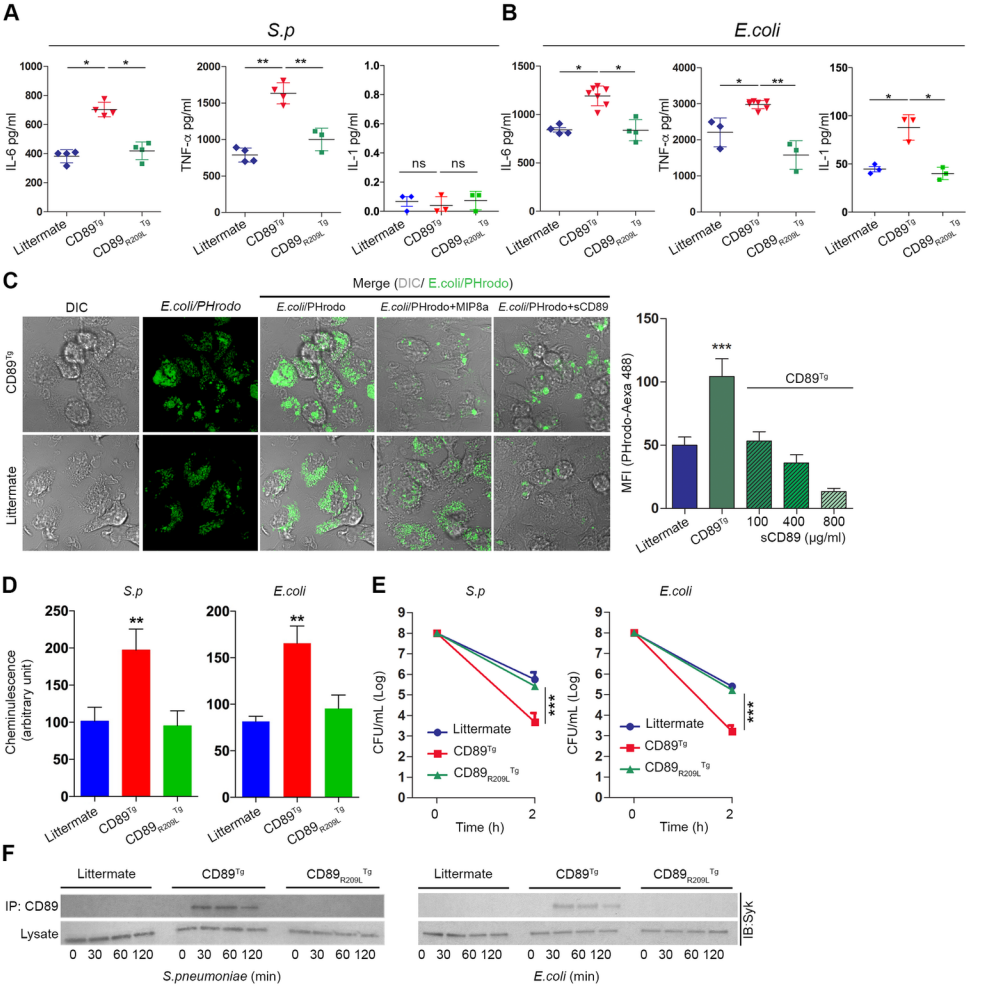
A
S.p
IL-6 pg/ml
TNF-α pg/ml
IL-1 pg/ml
ns
Littermate
CD89Tg
CD89R209LTg
B
E.coli
C
DIC
E.coli/PHrodo
Merge (DIC/ E.coli/PHrodo)
E.coli/PHrodo
E.coli/PHrodo+MIP8a
E.coli/PHrodo+sCD89
CD89Tg
Littermate
MFI (PHrodo-Aexa 488)
sCD89 (μg/ml)
D
S.p
E.coli
Cheminulescence (arbitrary unit)
E
CFU/mL (Log)
Time (h)
F
IP: CD89
Lysate
IB:Syk
S.pneumoniae (min)
E.coli (min)

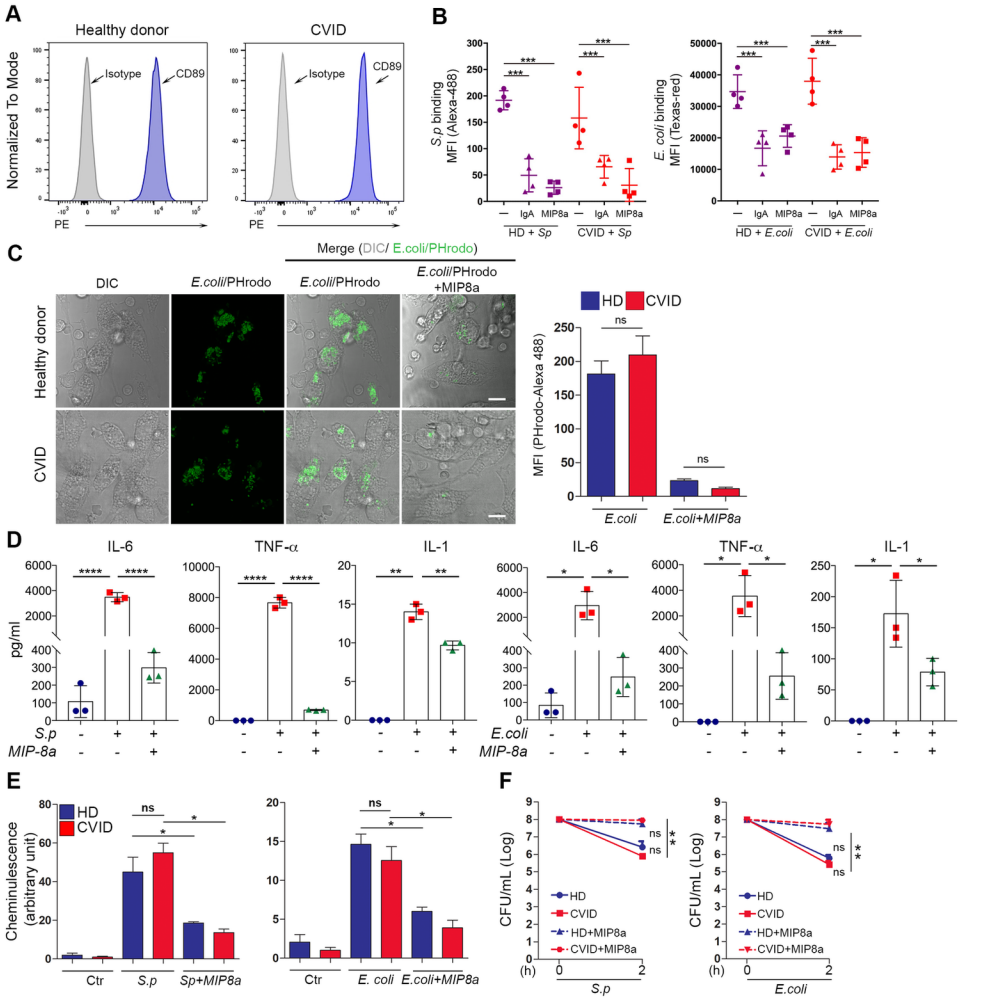
A
Healthy donor
CVID
Isotype
CD89
Normalized To Mode
PE
B
S.p binding MFI (Alexa-488)
E. coli binding MFI (Texas-red)
IgA
MIP8a
HD + Sp
CVID + Sp
HD + E.coli
CVID + E.coli
C
Merge (DIC/ E.coli/PHrodo)
DIC
E.coli/PHrodo
E.coli/PHrodo +MIP8a
Healthy donor
CVID
HD
CVID
MFI (PHrodo-Alexa 488)
ns
E.coli
E.coli+MIP8a
D
IL-6
TNF-α
IL-1
pg/ml
S.p
MIP-8a
E.coli
E
HD
CVID
Cheminulescence (arbitrary unit)
Ctr
S.p
Sp+MIP8a
E. coli
E.coli+MIP8a
F
CFU/mL (Log)
HD
CVID
HD+MIP8a
CVID+MIP8a
(h)
S.p
E.coli

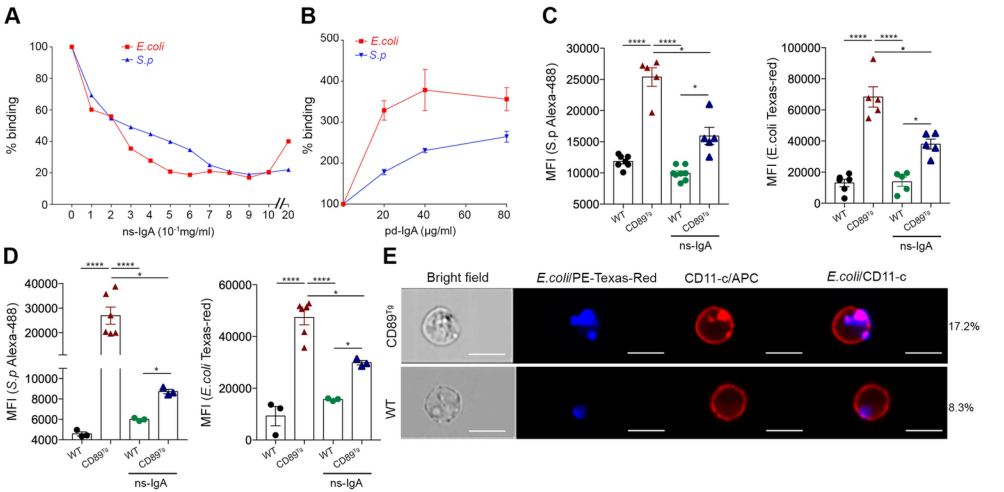
A
E.coli
S.p
% binding
ns-IgA (10-3mg/ml)
B
E.coli
S.p
% binding
pd-IgA (μg/ml)
C
MFI (S.p Alexa-488)
MFI (E.coli Texas-red)
WT
CD89tg
ns-IgA
D
MFI (S.p Alexa-488)
MFI (E.coli Texas-red)
WT
CD89tg
ns-IgA
E
Bright field
E.coli/PE-Texas-Red
CD11-c/APC
E.coli/CD11-c
CD89tg
WT
17.2%
8.3%

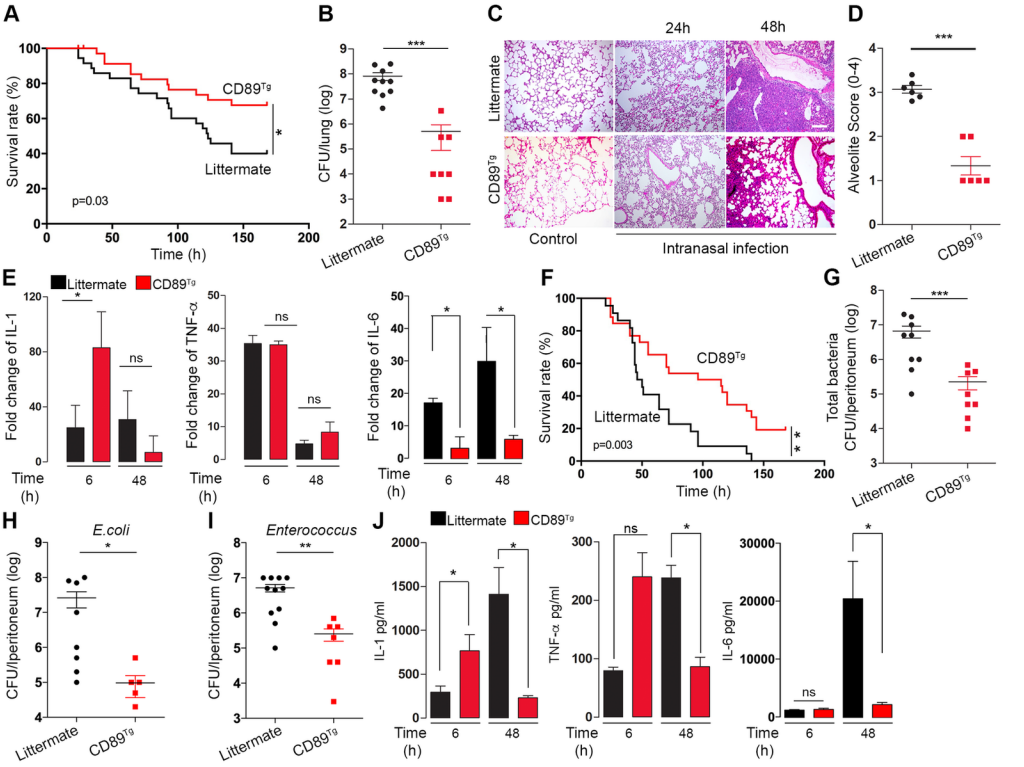
A
Survival rate (%)
CD89Tg
Littermate
p=0.03
Time (h)
B
CFU/lung (log)
***
Littermate
CD89Tg
C
24h
48h
Littermate
CD89Tg
Control
Intranasal infection
D
Alveolite Score (0-4)
***
Littermate
CD89Tg
E
Littermate
CD89Tg
Fold change of IL-1
Fold change of TNF-α
Fold change of IL-6
ns
Time (h)
6
48
F
Survival rate (%)
CD89Tg
Littermate
p=0.003
Time (h)
G
Total bacteria CFU/Iperitoneum (log)
***
Littermate
CD89Tg
H
E.coli
CFU/Iperitoneum (log)
Littermate
CD89Tg
I
Enterococcus
CFU/Iperitoneum (log)
Littermate
CD89Tg
J
Littermate
CD89Tg
IL-1 pg/ml
TNF-α pg/ml
IL-6 pg/ml
ns
Time (h)
6
48

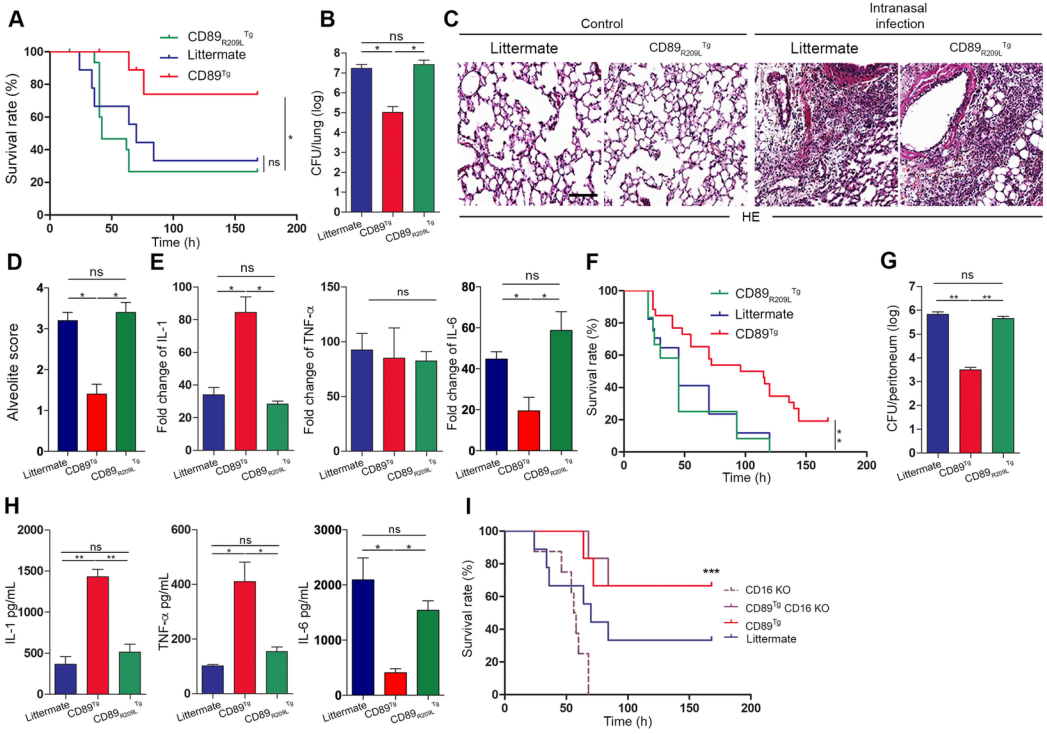
A
Survival rate (%)
Time (h)
CD89R209L Tg
Littermate
CD89Tg
ns
*
B
CFU/lung (log)
ns
Littermate
CD89Tg
CD89R209L Tg
C
Control
Intranasal infection
Littermate
CD89R209L Tg
HE
D
Alveolite score
E
Fold change of IL-1
Fold change of TNF-α
Fold change of IL-6
F
Survival rate (%)
Time (h)
G
CFU/peritoneum (log)
H
IL-1 pg/mL
TNF-α pg/mL
IL-6 pg/mL
I
Survival rate (%)
Time (h)
CD16 KO
CD89Tg CD16 KO
CD89Tg
Littermate

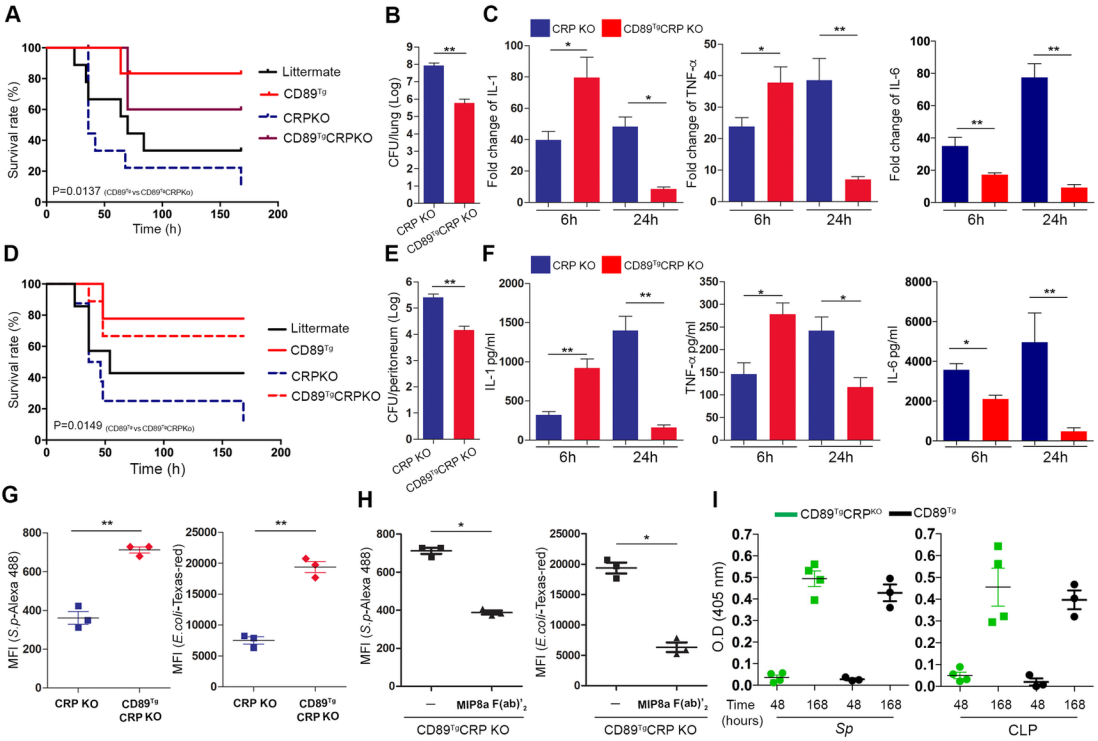
A
Survival rate (%)
Time (h)
Littermate
CD89Tg
CRPKO
CD89TgCRPKO
P=0.0137 (CD89Tg vs CD89TgCRPKo)
B
CFU/lung (Log)
CRP KO
CD89TgCRP KO
C
CRP KO
CD89TgCRP KO
Fold change of IL-1
Fold change of TNF-α
Fold change of IL-6
6h
24h
D
Survival rate (%)
Time (h)
Littermate
CD89Tg
CRPKO
CD89TgCRPKO
P=0.0149 (CD89Tg vs CD89TgCRPKo)
E
CFU/peritoneum (Log)
CRP KO
CD89TgCRP KO
F
CRP KO
CD89TgCRP KO
IL-1 pg/ml
TNF-α pg/ml
IL-6 pg/ml
6h
24h
G
MFI (S.p-Alexa 488)
MFI (E.coli-Texas-red)
CRP KO
CD89Tg CRP KO
H
MFI (S.p-Alexa 488)
MFI (E.coli-Texas-red)
–
MIP8a F(ab)'2
CD89TgCRP KO
I
CD89TgCRPKO
CD89Tg
O.D (405 nm)
Time (hours)
48
168
Sp
CLP

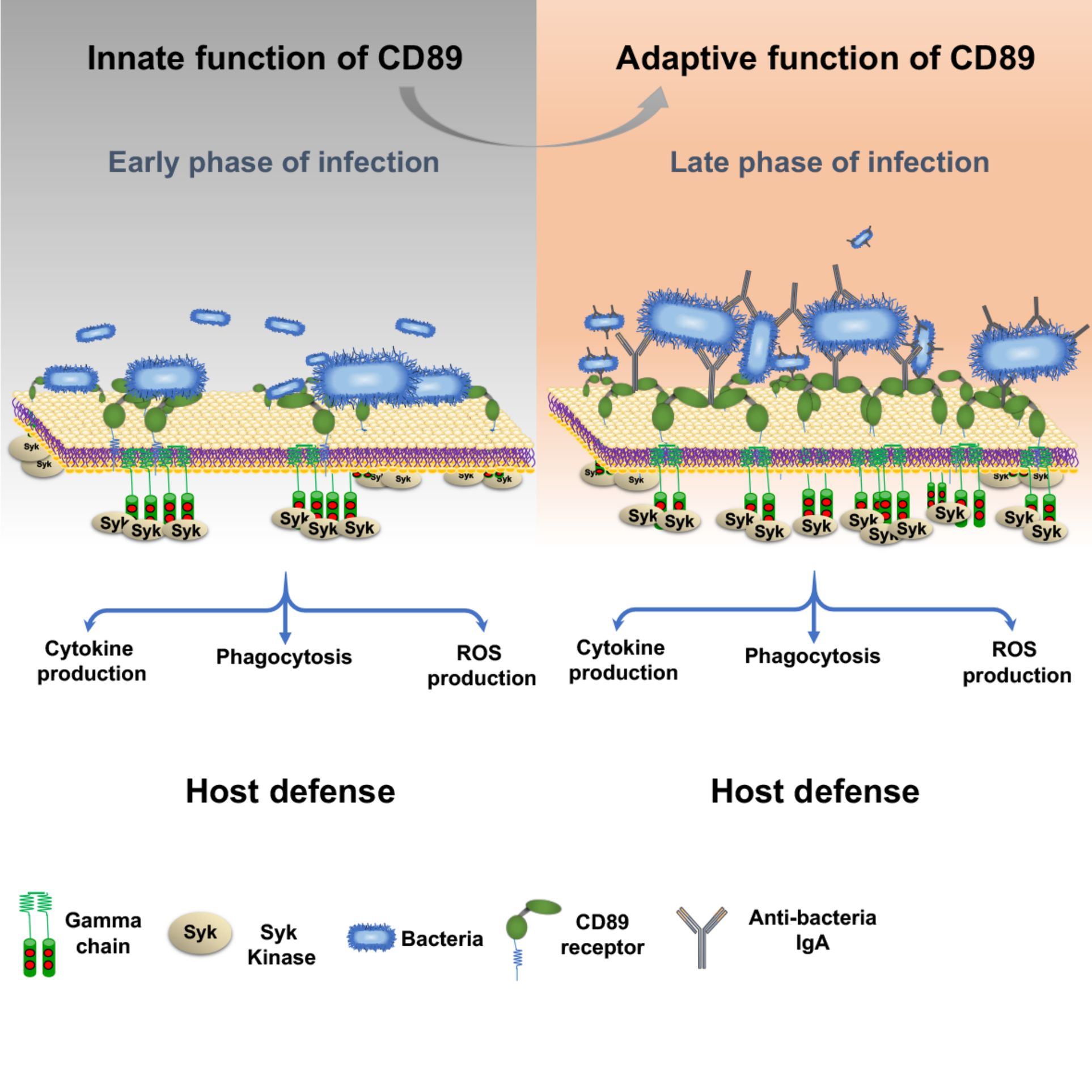
Innate function of CD89
Adaptive function of CD89
Early phase of infection
Late phase of infection
Syk
Cytokine production
Phagocytosis
ROS production
Cytokine production
Phagocytosis
ROS production
Host defense
Host defense
Gamma chain
Syk
Syk Kinase
Bacteria
CD89 receptor
Anti-bacteria IgA